Realisation of radiographic film dosimetry for IMRT QA at the Nepean Cancer Care Centre

A thesis submitted in (partial) fulfilment of the requirements for the degree of
Master of Applied Science (Medical and Health Physics)

Christopher J. Gehrke
Bachelor of Applied Science (Applied Physics)

School of Applied Sciences
College of Science, Engineering and Health
RMIT University
Melbourne AUSTRALIA
September 2010

Statement.

To the best of my knowledge the work in this thesis is original except where reference is made and no other person's work has been used without appropriate acknowledgement. The experimentation and analysis of data contained herein were produced from my own work with guidance based on medical physics literature and support from colleagues within the field. This thesis has not previously been submitted in whole or in part for any academic award to any Institute or University. The content of this thesis is the result of work carried out since the official commencement date of the approved research program.

Christopher J. Gehrke

September 2010

Acknowledgements.

The author would like to thank the Nepean Cancer Care centre for their financial support in purchasing consumables and permitting the use of experimental equipment needed for this project. The author thanks Shan Yau and Edgar Estoesta for their consultation during the early stages of the project and for their enthusiasm in initiating such a project. Thanks also to Trevor Ackerly and Anne Perkins for their valuable help and comprehensive knowledge during the written component of this work and to Rick Franich and Jeffrey Crosbie for their dedication in assuring the quality of the work was of an acceptable scientific standard.

The scientific writing component of this project proved most challenging and the author unambiguously recognises that without the help of the above-mentioned contributors this obstacle would have never been surpassed; their help was paramount and the author is indebted to them all.

Table of contents.

Summary 1

1 Introduction 4

1.1 Overview of the thesis 5

2 Background 7

2.1 Quality assurance in radiotherapy 7

2.2 Film dosimetry and associated uncertainties 8

2.3 Why use radiographic film? 11

2.4 The multileaf collimator 12

2.5 Radiographic film 14

2.6 Film processing using the AGFA HT-330 processor 16

2.7 Film digitising 19

2.8 Acceptance criteria 20

2.9 The need for independent QA of radiographic film dosimetry 23

3 Equipment 26

3.1 AGFA model Curix HT-330 film processor 26

3.2 DoseLab 26

3.3 ePin – An electronic fiducial utility 27

3.4 ImageJ 27

3.5 Kodak X-Omat V Ready Pack radiographic film 27

3.6 Nuclear Enterprises model 2571 and 2581 ionisation chambers 27

3.7 Philips Pinnacle treatment planning system 28

3.8 Polystyrene $(CH_2)_n$ phantom 28

3.9 Varian linear accelerators 29

3.10 Vidar model VXR-16 DosimetryPRO digitiser 30

3.11 Victoreen model densitometers 31

3.12 Victoreen Keithley model 35040 electrometer 32

4 Method 34

4.1 Digitiser characterisation 34

4.1.1 Light source uniformity 34

4.1.2 Light source constancy 36
4.1.3 Geometric accuracy 36
4.2 Film processor characterisation 36
4.3 Radiographic film characterisation 39
4.3.1 Base plus Fog 40
4.3.2 Dose rate dependence 41
4.3.3 Dose fraction dependence 42
4.3.4 Film homogeneity 42
4.3.5 Radiographic film energy sensitivity dependence 43
4.4 Error analysis 44
4.4.1 Film dosimetry uncertainty 45
4.4.2 Linac dosimetric uncertainty 46
4.4.3 Overall dosimetric uncertainty 46
4.4.4 Geometric uncertainty 46
4.5 DoseLab fluence comparison 47

5 Results and dicussion 48
5.1 Digitiser characterisation 48
5.1.1 Light source uniformity 48
5.1.2 Light source constancy 51
5.1.3 Geometric accuracy 53
5.2 Film processor characterisation 54
5.3 Radiographic film characterisation 57
5.3.1 Base plus Fog 57
5.3.2 Dose rate dependence 58
5.3.3 Dose fraction dependence 59
5.3.4 Film homogeneity 61
5.4 Error analysis 61
5.4.1 Film dosimetry uncertainty 61
5.4.2 Linac dosimetric uncertainty 62
5.4.3 Overall dosimetric uncertainty 62
5.4.4 Geometric uncertainty 62
5.5 Practical implications in the OD-to-dose calibration uncertainty 63
5.6 DoseLab fluence comparison 66

5.7 Further discussions 67

6 Conclusion 69

7 Glossary 72

8 References 76

List of figures.

Figure	*Section*	*Description*	*Page*
1	2.4	Varian multileaf collimator (MLC) carriage illustration	12
2	2.4	MLC leaf illustration	13
3	2.4	Step and shoot IMRT field leaf segments	14
4	2.5	Kodak radiographic film layer composition	15
5	2.8	NAT flowchart	21
6	2.8	Profiles illustrating the use of the DTA criterion	22
7	3.6	An image of a NE model 2571 ion chamber	28
8	3.8	An image of sectional solid water sheets	29
9	3.9	An image of a Varian model 21EX linear accelerator	30
10	3.10	An image of a Vidar VXR-16 DosimetryPRO digitiser	31
11	3.11	An image of a Victoreen model 07-424 densitometer	32
12	3.12	An image of a Keithley model 35040 electrometer	33
13	4.1.1	Film digitising orientation using the Vidar digitiser	35
14	4.2	OD-to-dose calibration; ion chamber and film arrangement illustration	37
15	4.3.2	Dose rate dependence; ImageJ region of interest screenshot	42
16	5.1.1	Light source uniformity; horizontal profiles of the UST	48
17	5.1.1	Light source uniformity; vertical profiles of the UST	49
18	5.1.1	Light source uniformity; an image of feed roller damage during digitising	51
19	5.1.2	Light source constancy; horizontal profiles of the UST over several months	52
20	5.1.2	Light source constancy; distribution of values	53
21	5.2	Film processor characterisation; OD-to-dose curves	54
22	5.3.1	Base plus Fog; corrected and uncorrected uniformity correction profiles	57
23	5.3.4	Film homogeneity; profiles of Base plus Fog from two film batches	61
24	5.5	DoseLab interactive profiles between two OD-to-dose calibrations	64
25	5.5	Error analysis; film processing uncertainty histogram	65
26	5.6	DoseLab fluence comparison	66

List of tables.

Table	*Section*	*Description*	*Page*
1	2.9	Published film uncertainties in radiotherapy beams	25
2	3.1	Specifications for the AGFA model HT-330 film processor	26
3	4.2	OD-to-dose calibration; ion chamber and film arrangement linac settings	38
4	4.2	OD-to-dose calibration; ion chamber and film arrangement linac Jaw settings	38
5	4.2	Densitometer manufacturer specifications	38
6	4.2	OD-to-dose calibration; ion chamber readings for one location	39
7	5.1.3	Geometric accuracy; horizontal direction	53
8	5.1.3	Geometric accuracy; vertical direction	53
9	5.2	Film processor characterisation; differences between OD values	55
10	5.3.2	Dose rate dependence; radiographic film results	58
11	5.3.2	Dose rate dependence; ion chamber results	58
12	5.3.3	Dose fraction dependence; radiographic film results for 200 cGy/min	59
13	5.3.3	Dose fraction dependence; radiographic film results for 600 cGy/min	60
14	5.3.3	Dose fraction dependence; ion chamber results for 200 cGy/min	60
15	5.3.3	Dose fraction dependence; ion chamber results for 600 cGy/min	60
16	5.4.1	Film dosimetry uncertainty; radiographic film dosimetry uncertainties	62
17	5.4.4	Radiographic film geometric uncertainties	63

Summary.

The goal of this project was to determine the viability of using radiographic film for patient specific quality assurance (QA) at the Nepean Cancer Care centre. To determine if such a process would succeed, the accuracy and precision of radiographic film as a 2D radiation detector was quantified. This required the characterisation of three main areas: film digitising, film processing and defining the unique characteristics of radiographic film.

Radiographic film is one verification tool used in three-dimensional conformal radiotherapy (3DCRT) and physicists use this film as a relative dosimeter in regular quality assurance. Specifically, this study aims to establish the viability of using Kodak[a] X-Omat V radiographic film as an absolute dosimeter in evaluating delivery accuracy.

Several instruments were utilised during this study. An AGFA[b] film processor was used to transform an exposed film into the visible darkening needed to measure optical density (OD). A Vidar[c] film digitiser and two Victoreen[d] densitometers were used to measure the magnitude of film OD. A Varian[e] linear accelerator (linac) was used to expose film. Philips[f] Pinnacle treatment planning system (TPS) was used to calculate simulated treatment plans and compute 2D intensity (fluence) maps representative of radiation treatment beams (fields). DoseLab[g] was used to compare fluence maps created from simulated and measured linac field data.

Simulated patient data was measured using virtual patients (phantoms). A Varian model 21EX linear accelerator with a Millenium multileaf collimator (MLC) produced the desired measured data. DoseLab was utilised to correlate image data created in Pinnacle and measured with film. Uncertainties originating from film, film processing, film digitising, mechanical and theoretical uncertainties were assessed.

[a] Eastman Kodak Company, Rochester, New York, USA.
[b] AGFA-Gevaert N.V., Mortsel, Belgium.
[c] Vidar Systems Corporation, Hendon, Vancouver, USA.
[d] Victoreen Inc., Cleveland, Ohio, USA.
[e] Varian Medical Systems, Palo Alto, California, USA.
[f] Royal Philips Electronics, Eindhoven, the Netherlands.
[g] DoseLab is a set of software programs developed by Nathan Childress as part of his PhD project. It can be used for quantitative comparison of measured and computed radiation dose distributions and is available as freeware from http://doselab.sourceforge.net/.

A film digitiser was used to create digital images, which could be analysed from plotted data. When digitising, three areas were assessed: light source uniformity, constancy, and geometric accuracy. Light source uniformity and constancy were measured using unexposed (blank) radiographic film. This blank film created calibration templates that served as standards that could characterise the digitising process. Measurement of pre and post digitising were defined from these templates.

Film processing characterisation was examined from film exposures made over a period of five months. Two different digitising instruments were used to measure this exposure variation: a Victoreen densitometer and a Vidar digitiser.

For defining film characteristics, four features were assessed: Base plus Fog, dose rate dependence, homogeneity and dose fraction dependence. Base plus Fog was defined by measuring the optical density of blank film. A linear accelerator was used to expose film at different dose rates and the differences in film optical density were measured to assess film dose rate dependence. Fraction dependence was measured in a similar way however fractions of an exposure were compared to whole exposures. Film homogeneity was assessed by comparing the variation in optical density on blank films arising from different manufacturing batches.

The concluding analysis involved comparing computed (TPS) and measured (linac) fields. The computed field was created automatically by a feature in Pinnacle and exported as a text file. The measured field was created by using the simulated planned data to expose radiographic film. After indentifying uncertainties in the process of creating a measured field, the resulting images (TPS and linac) were correlated and evaluated using DoseLab. The data were analysed for magnitude and displacement differences taking into consideration the uncertainties involved when using radiographic film at the centre.

The greatest uncertainty throughout the evaluation was measured for the optical variation in film processing that yielded a derived uncertainty of 11%. The digitiser's light source uniformity was in the order of 5% across the length of the device and during scanning the variation in the output was 1.5%. Constancy of the light source was approximately 0.7% and the geometric accuracy was equal to or less than 0.8 mm adding to a combined geometric accuracy of 0.97 mm. The variation in optical density

from dose rate or fraction dependence proved inconclusive since film processing variations outweighed any variations due to these dependencies. Minimal dose rate and fraction dependence were observed for the film and minimal variations (<0.2%) between film manufacture batches were recorded.

The expected film dosimetry accuracy for Kodak X-Omat V film under ideal conditions as recommended by the American Association of Physicists in Medicine (AAPM) Task Group (TG) 69[1] is 4% or 3 mm. In comparison, the Nepean Cancer Care centre's dosimetric accuracy was far greater (11%) and as a result the procedures adopted in this work were not implemented. To improve accuracy consideration towards the purchasing of a film processor capable of accurately maintaining processing temperature, chemistry, and processing speed is advised or consideration towards other film manufacturing types such as radiochromic films should be considered.

1 Introduction.

Radiation Oncology (radiation therapy or radiotherapy) is the treatment of cancer using ionising radiation. Radiation oncology is composed of various speciality disciplines of which the radiation oncology physicist is a part. One of the roles of the radiation oncology physicist is to ensure through measurements that the prescribed treatment matches what is actually delivered. Kutcher et al. (1994)[2] in their report to the AAPM define the responsibilities of the radiation oncology physicist as, "*primarily and professionally engaged in the evaluation, delivery, and optimization of radiation therapy.*" Fraass et al. (1998)[3] describe quality assurance (QA) specific to this role, "*the radiation oncology physicist shall be primarily responsible for the design and implementation of the QA program for treatment planning.*" Furthermore, "*the radiation oncology physicist determines the local QA program for treatment planning, including the tests to be performed, tolerances, and frequency of the tests.*"

The measurements associated with the role of a radiation oncology physicist for the purpose of QA cover a wide dynamic range. The importance of this QA stems from the requirements of treatment planning, which aims to achieve doses within tight tolerances and thus ensure adequate coverage of cancer near or around healthy tissue. If it is not ensured through rigorous QA that these requirements are met, healthy tissue may receive lethal and unwarranted doses. Additionally, it is widely recognised that over-dosage may be lethal to the patient and under-dosage may leave the cancer viable in which case the patient is not cured. One such type of treatment that aims to achieve adequate coverage of cancers near and around healthy tissue is Intensity Modulated Radiation Therapy (IMRT).

IMRT is a supplement to three-dimensional conformal radiotherapy whereby it additionally shapes the delivered doses by modulating the dose intensity across each field.[4] IMRT is a specific type of radiation therapy that aims at conforming radiation dose to a defined target volume while also minimising healthy tissue dose. IMRT requires more stringent quality assurance than traditional external beam radiation therapy. In implementing IMRT in their own department, a physicist is faced with the task of adapting specific tools and dosimetric techniques to achieve the stringent demands of IMRT QA. Hence, the aim of this work was to implement radiographic film dosimetry, a technique already used by physicists for general QA, into IMRT QA at the Nepean Cancer Care centre. For this to occur, the uncertainties associated with equipment located at the centre for using radiographic film was determined along with the uncertainties associated with IMRT relevant to film dosimetry. These include the characterisation of a film digitiser and processor, and defining film manufacture and response

properties. Film processing, film manufacturing reproducibility and construction were determined and for IMRT and film specific uncertainties related to IMRT, film dose rate and dose fraction dependence were investigated.

1.1 Overview of the thesis.

Chapter 2 introduces radiation therapy, radiation therapy physics and film dosimetry. This chapter describes the purpose of QA in this area and the uncertainty that arises when using film for IMRT QA. Multileaf collimators (MLC) are described, image formation from film processing, and film digitising including their uncertainties are explained. Film dosimetry evaluation criteria (acceptance criteria) and how they influence uncertainty are also described. Chapter 3 documents the apparatus used in the study.

Chapter 4 details the methods used to characterise the uncertainty of film dosimetry, culminating in a description of the procedure to check an IMRT plan with film dosimetry. This includes the characterisation of a film digitiser and processor, and defining film manufacture and behaviour properties. Characterisation of the film digitiser included the examination of its light source and image manipulation process. Film processing reproducibility was measured to examine the uncertainty in chemical reaction variability during processing. Manufacturing reproducibility, construction, dose rate and dose fraction dependence were investigated for defining radiographic film's inherent characteristics and practicality of use.

Chapter 5 lists the results from the characterisation of the digitiser, which shows the variation of light intensity across the length of the extended source, the constancy of the light intensity over five months, and the geometrical accuracy of the digital reproductions created when digitising film. The film processor is also characterised from the differences between graphs of optical density versus dose and comparisons between radiographic and radiochromic films. The chapter also includes the results from film characterisation; measuring the background dose attributed to film's opacity (Base plus Fog) and by assessing field variations that occur in IMRT fields that can influence the accuracy of film measurements i.e. dose rate and cumulative dose variations (fraction dependence). The variations between two film batches are also contained in this chapter. The chapter concludes with an analysis and calculation of the overall uncertainty from each film processing step and illustrates the assessment process with a

comparison of IMRT fields (calculated and measured) using radiographic film dosimetry uncertainties specific to the centre.

Chapter 5 also discusses the variation of light intensity within the digitiser and how it influences measurements made with film. It also illustrates the general problems when using film digitisers. The uncertainty in film processing is discussed from the variation in optical density to relatively consistent dose data and how these influences dose as measured during IMRT radiographic film dosimetry. Chapter 5 also discusses further some of the key implications identified during this study specific to the centre.

Chapter 6 concludes the investigation by highlighting the main areas of this project regarding the implementation of radiographic film for IMRT QA at centre. The chapter also identifies what steps are required to further improve procedures for IMRT QA and highlights concepts for future studies. Chapter 7 and 8 refer to a glossary of terms and a list of references.

2 Background.

This chapter establishes that accurate quality assurance is required for the curative and beneficial administration of intensity modulated radiotherapy treatment to the patient. To achieve this, it is necessary to describe the process of forming an image on radiographic film, from radiation created in a linear accelerator, for the purpose of radiotherapy quality assurance. Coupled with this is a need to characterise uncertainties associated with methods and equipment. These include the uniformity and constancy of light sources for digitising films and the accuracy in reproducing displacements on digital images. The method of film processing and how chemistry, heat and time impact on image formation and consequently image quality must also be considered. In addition, radiographic film properties are characterised including Base plus Fog, dose rate and fraction dependence, and manufacturing reproducibility. This chapter explains radiotherapy in a generalised way, it explains film dosimetry and discusses the criteria used for a treatment field comparison, it explains why radiographic film was chosen and why there was a need to characterise a known detector's response from existing published literature.

2.1 Quality assurance in radiotherapy.

External beam radiotherapy is a curative medical procedure targeting cancer. It utilises X-rays that destroy cancer cells from direct interaction or indirectly by producing free radicals. When radiation interacts with matter, the biological damage depends on the amount of energy absorbed, which is measured in Joules per kilogram (J/kg) and is represented by the unit Gray (Gy).

Ionising radiation breaks down the nucleus of cells mainly through damage of deoxyribonucleic acid (DNA). DNA is a constituent of chromosomes and the carrier of genetic information. Two causalities arise from the interacting radiation. For direct harm, atoms of the target cell are ionised or excited leading to a chain of physical and chemical events that produce the biological damage. For indirect harm, the damage occurs when the interactions with water produce free radicals such as hydroxyl (OH^-) that break chemical bonds. The resulting harm to cells is either a loss of function, reproductive failure, cell death or no effect. The type of effect depends on the magnitude of radiation, its ionising potential, its intensity, the interaction time, the cell type and which reproductive phase it is in and the tissue or organ type.

To deliver Intensity Modulated Radiation Therapy (IMRT), therapeutic X-rays are produced using a radiotherapy linear accelerator (linac). The radiation produced by a linac is shaped with blocking devices to create fields that better conform to the shape of the target volume. The radiation may be directed around a cylindrical volume of approximately 20 cm radius in a 360-degree arc via a rotation mechanism. The treatment technique can conform to almost any shape, restricted in size only by mechanical limits. For the treatment to achieve a complication free curative outcome it is considered that careful variation of radiation direction and irradiated volume is required. This is known as three-dimensional conformal radiotherapy (3DCRT). A treatment that has the potential to surpass the clinical effectiveness of 3DCRT is a method known as Intensity Modulated Radiation Therapy (IMRT). IMRT utilises a dynamic shielding system comprised of wafer-like shields called a Multileaf Collimator (MLC), which is capable of creating improved conformal shapes.

When using ionising radiation it is essential that a quality assurance protocol is in place to ensure the, "*protection of people and the environment from the detrimental effects of exposure to ionizing radiation*."[5] For example, to guard against errors that occur from mechanical and electric drift, computational anomalies, and data transfer mismatch. There is also a need to understand the uncertainties involved so that excessive doses to healthy tissues are avoided.

This project aims to assess the viability of using Kodak X-Omat V radiographic film to implement an independent form of IMRT verification. In particular, it verifies the current treatment planning system (TPS), Pinnacle version 7.6, independently using phantoms and radiographic film. The project studies the practicality of using film for verifying simulated patient treatment plans. The main focus of the work described here is to determine if the uncertainty involved in using radiographic film is sufficiently low that a comparison of computed (TPS) and measured (linac) dose achieves sufficient accuracy for verification purposes[6-24] and subsequently quality assurance.

2.2 Film dosimetry and associated uncertainties.

Multiple authors[7,8,12,14,25-29] conclude that more stringent quality assurance is required for IMRT than for conventional radiotherapy. This is due to numerous small field sizes, high dose gradients and penumbral regions present in IMRT fields, which is difficult to verify with accurate dosimeters.[7] Penumbral regions are difficult to measure because of detector volume averaging and large errors can occur.[7] In IMRT,

each field is created by a number of smaller fields and thus each field consists of numerous penumbral regions that are a great deal more difficult to verify. In addition, there exists a challenge of calculating the dose distributions associated with an MLC including the effects of rounded leaf ends, which increases penumbral effects and alters energy fluence and thus dose deposition leading to general errors of 3% and 3 mm, up to 26.6% if not corrected, even after the phenomena is properly accounted for in planning calculations.[30] The so called tongue and groove effect[30,31] or interleaf transmission,[32] which can cause errors of 28.4% with a penumbra (FWHM) of 4.2 mm,[31] and intraleaf transmission[30,32] that can also cause errors of 3% and 3 mm.[30] Leaf displacement[33] errors also result in inaccuracies when different penumbras are cast depending on the position of each leaf in the MLC with respect to the displacement of the leaf from the centre of the device. Butson et al. (2003)[32] measured a difference of 0.2 mm in the penumbra of the leaf end between a 15 cm offset and a zero offset. Whereas, Huq et al. (2002)[34] using a similar measurement recorded a 0.4 mm difference.

The problems arising from the MLC are discussed in more detail in section 2.4. As a consequence of the above-mentioned problems several authors[14,17,20,35] recommend using a 2D dose verification tool to properly measure IMRT fields. Film is capable of measuring in 2D and has superior spatial resolution to all other detectors such as diodes, ionisation chambers, electronic portal imaging devices and thermoluminescent dosimeters.[7,17,19,20,24,26,27,36,37]

In recognition on the difficulty of using radiographic film for IMRT the American Association of Physicists in Medicine (AAPM) have appointed a task group (TG) 69[1] to consolidate these difficulties. The AAPM report was published several years after this work however the problems identified in the AAPM report match those addressed here. To have a large organisation like the AAPM address the use of radiographic film for IMRT QA gives evidence that a need was also apparent for the Nepean Cancer Care centre. In addition, most of the referenced literature in the AAPM report is dated prior to 2005, the same year the practical component of this study was complete, and their references match those referenced in this study.

The AAPM report is divided into six sections: (i) the characteristics of silver halide films, (ii) practical aspects of film processing, (iii) detection equipment, (iv) dosimetric characteristics of commonly used films and phantoms, (v) film calibration protocol, and (vi) clinical applications. Section (i) describes the principles of film processing, image formation, optical density, the dependence of optical density on

processing conditions, the relationship between absorbed dose and optical density, energy dependence, dose rate and spatial resolution. These characteristics are also reproduced in this study under sections 2.6, 4.2 and 5.2. Section (ii) of the report describes the factors that influence film processing such at the developer, fixer, washing and drying, chemistry control, processing time, and temperature control. These characteristics and effects are quantified in section 2.6 of this study. In addition these two sections of the AAPM report describe acceptance and commissioning, and quality assurance of film processors. Similar documentation was also addressed for the centre although omitted from the body of text, which explains the physical processes involved rather than the physical procedures themselves.

Section (iii) of the AAPM report lists detector equipment used for film dosimetry. The report describes the characteristics of 2D digitisers like the Vidar (sections 3.10, 4.1 and 5.1) and point dosimeters (sections 3.11 and 5.2). They address problems with 2D digitisers such as geometric accuracy (sections 4.1.3 and 5.1.3) and light source uniformity (sections 4.1.1 and 5.1.1). They also describe dose calibration procedures (sections 4.2 and 5.2) and light scatter artefacts (section 5.1.1).

Section (iv) of the report documents the dosimetric characteristics of commonly used films and phantoms; it lists the types of films available and their optical density range, and phantom materials. This is also addressed in this study under sections 2.3 and 2.5. Their recommendations refer only to tissue-equivalent phantoms like those used for this study (section 3.8). Section (v) explores the various film calibration geometries i.e. film vertical or horizontal with respect to the direction of the beam. Recommendation is given to prick the film packages to release air sealed inside and that the experiment should be accurately reproducible. Film pricking was adopted in conjunction with digital pricking (section 3.3 and 4.5) for image correlation and one film exposure procedure was adopted using predefined phantoms dimensions to ensure setup reproducibility (section 4.2 and 5.2). Section (vi) lists the clinical applications of film for which intensity modulated radiotherapy is one. Further analysis of the problems associated with using radiographic film for IMRT QA is continued throughout this chapter.

It should be noted that the AAPM TG 69[1] report was published (2007) several years after the experimental component of this work was complete (2005). The AAPM report is now considered the most important document relevant to radiographic film dosimetry in this discipline. Even though the AAPM report was published after this work the majority of references made in the report are no older

than 2005 (only 3 publications in 109 were published in 2006) and those references used by the AAPM are the same as those referenced here. Hence, the sourced data are very similar for both studies. In addition, the report emphasises the recognition on the difficulty of using radiographic film for specialised types of 3DCRT and thus validates the need and purposes of this study for this centre.

2.3 Why use radiographic film?

There are two alternatives to using radiographic film: Extended Dose Range (EDR) and radiochromic films. Olch (2002)[12] suggests, "*IMRT QA demands that film dosimetry be able to accurately measure dose between about 5 and 250 cGy over a wide range of depths, beam directions and irradiated areas.*" IMRT at the Nepean Cancer Care centre does not currently have fractions greater than approximately 2 Gy, which is delivered with five to seven fields. The validity of EDR film was considered. The nominal sensitivity of EDR film as stated by Kodak (2005) extends between 25 to 700 cGy. EDR film is less suitable for each field because the centre's IMRT dose range is between 0 to 120 cGy. Therefore, EDR film would be less sensitive for these fields than Kodak X-Omat V (XV) film because its sensitivity range is between 5 and 200 cGy.[h] Stern et al. (2004)[26] suggest that XV film, "*has a response range of 0.04-1 Gy and a saturation exposure of 2 Gy.*" Danciu et al. (2001)[15] state, "*the Kodak film can be irradiated to high doses up to 2 Gy, reaching an optical density equal to 3, without being saturated.*" Cheng and Das (1996)[37] recommend the saturation density for Kodak films is approximately 3.5. Thus, XV film is more suitable than EDR for this range.

Since EDR film is not sensitive enough to measure IMRT fields an alternative would be to escalate the dose for each field. Dose escalation involves multiplying the prescribed dose for each field by an integer number. The multiplicative escalation can be compensated for by dividing through by a scaling factor at some other stage. Scaling implies the relationship between dose and optical density for the EDR film is linear. Dose escalation also implies that the MLC will generate identical energy and intensity fluence at different dose magnitudes. These two implications would require further investigation and add complexity to already complex problem. In addition to dose scaling, this creates a new plan that deviates from the original and consequently makes the evaluation of the original plan more difficult by introducing another step with another uncertainty. Consequently, introducing EDR film would add more complexity and greater uncertainty to the process. Therefore, in an effort to minimise uncertainties EDR film was not considered for the evaluation.

[h] Eastman Kodak Company, Rochester, New York, USA (2005).

Radiochromic film was considered as a substitute for radiographic film. However, the defining reason as to why radiochromic film was avoided was its price and availability. At the time of this study, the price of radiochromic film was approximately AU$50 per sheet of size 12.7 cm × 12.7 cm. For the centre's QA program, this can result in one sheet per field totalling some 14 beams and thus 14 sheets at a price of AU$700 for each patient. In addition, some fields are too large for this sized film which would require more film and thus incur more expense. Radiochromic film can perform film dosimetry though the centre could not justify the cost.

2.4 The multileaf collimator.

The multileaf collimator (MLC) as the name suggests is a collimating device comprised of many wafer-like radiation shields (leaves). Like radiation therapy shielding in general, its purpose is to partially or fully attenuate a radiation field to create dose variations that would otherwise be unattainable.

A depiction of one half of an MLC is illustrated in figure 2. Shown is the rounded end design of each leaf, which is compensatory for the device travelling along a perpendicular line rather than an arc from a diverging radiation source.

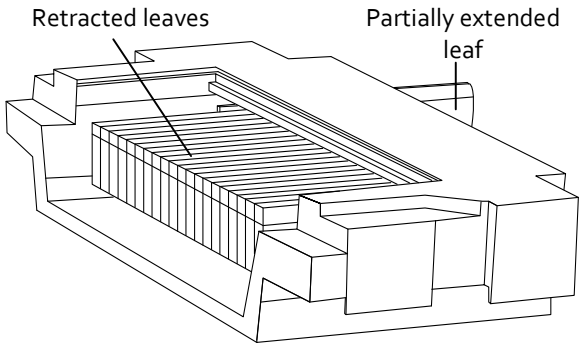

Figure 1. Illustration of the leaves contained in a Varian MLC. The MLC is comprised of two opposing carriages that accommodate individual leaves. Each leaf can extend and retract just like each carriage. Shown here is one partially extended leaf on one carriage. Each leaf has its own motor, not shown, and can move in and out separately from adjacent leaves on the same carriage.

Multileaf collimators differ in design depending on model and vendor.[37] The function of an MLC remains the same but engineering constraints cause each model to behave uniquely which creates a unique field defining environment. Some types of MLC move by retracting or extending along an arc while others follow a straight line. The Varian Millenium MLC leaves follow a straight line and consequently have rounded leaf ends to reduce penumbral width that arise at large field sizes due to beam divergence. A particular trait of the MLC is overlap between adjacent leaves in the same carriage, which is called the Tongue and Groove effect, and can be seen from the side view illustration of an MLC leaf in figure 2. In this situation, the tongue of one leaf fits into the groove of an adjacent leaf to reduce radiation leakage. The radiation leakage resulting from transmission between adjacent leaves is called Interleaf transmission and the radiation leakage through each leaf is called Intraleaf transmission. Radiation interactions resulting from the transmission through rounded end of a leaf is called Leaf End transmission. The magnitude and amount of radiation originating from the MLC depends on the design of the MLC, the position of the leaves, their size and the energy of the radiation the MLC is collimating.

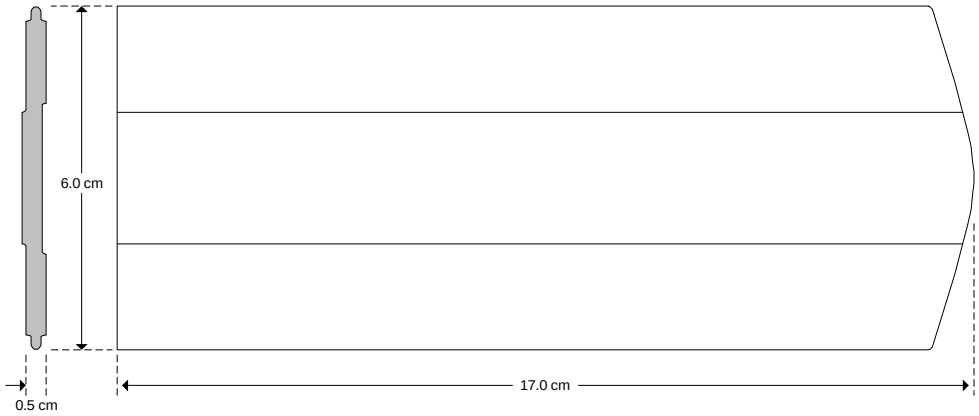

Figure 2. Illustration for one leaf contained in the MLC. Shown is the rounded leaf end (pictured right of the image) and a side view of the leaf showing the tongue and groove design.

One reason why this specific radiation leakage is of concern when using an MLC is the ability for a treatment planning system to simulate dose accurately.[38] Depuydt et al. (2001)[39] document a limitation of their planning system (Varian Helios Cadplan), which applies a single average 2% transmission to correct for all types of leaf transmission. Their measured data showed a variation from 1.5 to 2.2%, which contributed to the error in their QA evaluation. Dogan et al. (2002)[11] also made measurements for their MLC finding approximately 1.5% transmission. The radiation leakage formed by

the MLC is complex and is one of the reasons why analysis of dose estimations from simulated patient treatments requires stringent QA.

Varying the MLC position multiple times during the exposure of a radiation field can produce concave dose intensity distributions like the one shown in figure 3. Figure 3 is a simplistic illustration of the variation in intensity that can be created with several fields within fields. This specific type of treatment is referred to as intensity modulated radiotherapy.

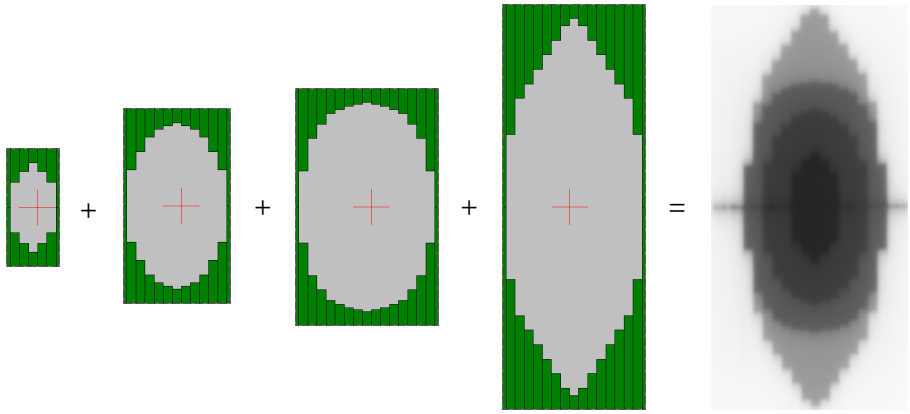

Figure 3. Illustration of the dose distribution created from an IMRT field. Four MLC leaf segments, fields in fields, are shown. The green rectangles display the position of each leaf as if seen by the radiation source. The completed exposed field is shown on the right of the image, which is a result of the combination from the four fields exposed with the same amount of radiation. The different shades of grey on the completed image show the change in intensity received by the film.

2.5 Radiographic film.

Kodak X-Omat V radiographic film was used for this project. It is a relatively low speed, dual sensitive layer flexible film with three coatings on each side excluding the supportive layer. The outer-most layer is made from gelatine, which serves as a protective sheath. Above the supportive layer rests an adhesive coating for an emulsion layer. Figure 4 shows the composite layers.

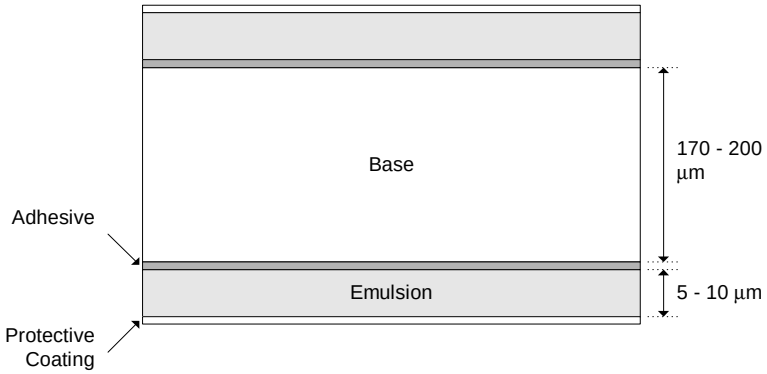

Figure 4. Illustration for the layers contained in Kodak Ready Pack XV radiographic film. Image adapted from Kron (1999)[18] and Heggie et al. (2001).[40]

The emulsion layer consists of silver halide and gelatine. The gelatine supports heterogeneous silver halide crystals distributed homogenously throughout the layer. The silver halide is composed of silver bromide (AgBr) and iodine. The mixture is between 1 to 10 percent iodine with the remainder composed of AgBr. Silver halide is suspended in the gelatine as small crystals with size ranging in the order of a few micrometers.

Kodak supplies the radiographic film in an airtight packet. The package exterior is an orange coloured paper with a density of approximately 160 grams per square meter (gsm). Adjacent to these layers and in contact with both sides of the film is a cellular composite layer similar in thickness and composition to regular copy paper of approximately 80 gsm. The exterior package for each film eliminates the need for loading cassettes and prevents visible, ultraviolet and infrared radiation from reaching the film. However, X-rays are capable of penetrating the protective cover and exposing the film which eliminates the need for light-tight devices.

When incident radiation such as X-rays interacts with the silver bromide a chemical reaction occurs. Free electrons and ions are formed. Equation 1 describes this process.

$$AgBr + photon \rightarrow Ag^{+} + Br^{-} + e^{-} \qquad [1]$$

During this reaction, bromide ions (Br^-) are absorbed by the gelatine although the reaction is reversible and the bromide may recombine with silver ions (Ag^+). Electrons that are released are free to move in the silver halide lattice. However, they are trapped within imperfections (sensitivity specks) located within the halide crystal. The trapped electron attracts positively charged Ag^+ and recombination occurs forming a silver atom. This process is termed nucleation and is described by equation 2. Growth around the sensitivity speck continues until the crystal becomes stable against recombination.[40]

$$Ag^+ + e^- \rightarrow Ag \qquad [2]$$

The physics of exposing a film and creating an image is complicated. Several authors[41,42] explain the image formation where ion pairs are formed within the silver halide lattice that attract interstitial ions and bond to form silver atoms. An exposed film viewed by eye would appear unexposed until the film undergoes processing. After processing, areas on the film exposed by radiation can be viewed by eye and appear darker than the surrounding area. The darker the film the more radiation was incident. The amount of radiation can be defined by the darkness of the film, quantified as its optical density.

2.6 Film processing using the AGFA HT-330 processor.

The transformation of an unexposed film to form a dark visible image requires two chemicals, a developer and a fixer. The developer assists in producing a chemical reaction in exposed radiographic film. The AGFA G138[i] three-part developer produces the chemical reaction needed to convert silver bromide to silver on and around a latent image centre. Some of the ingredients include hydroquinone, acetic acid and diethylene glycol. Acetic acid is used as a pH buffer and hydroquinone as a reactant for the silver bromide. Diethylene glycol acts as an inhibitor that lessens background development or so called Fog.

Time and temperature are critical parameters in the development stage. The developer will continue to reduce unexposed silver halide crystals indefinitely if given the opportunity. Temperature acts as an accelerant to the development reaction rate. To ensure the developer acts in a reproducible manner the AGFA model HT-330U film processor changes both time and temperature simultaneously. The

[i] AGFA G138i three part universal developer

processor monitors the throughput of film and the use of developer and fixer to ensure enough concentration of each chemical is available and automatically adjusts the concentration as needed. Higher temperatures result in shorter processing times to achieve the same result. Developer temperature ranges from 25°C to 39°C. During this study, all films where processed at 2 minutes and 34°C.

Fixing takes place after development. The AGFA G334 two-part fixer[j] rinses the undeveloped AgBr from the emulsion such that only silver crystals remain. These crystals form the visible or dark image. Among some of the ingredients contained within the fixer are aluminium sulphate and acetic acid. Equation 3 describes the chemical process of image formation.

$$QH_2 + 2AgBr \rightarrow Q + 2Ag + 2H^- + 2Br^- \qquad [3]$$

The chemical reaction of hydroquinone with AgBr produces: quinine, silver, ionic hydrogen and bromide ions. Aluminium sulphate is used as a preservative to reduce decomposition of the fixer. A quartz lamp dries the film after wet processing.

The uncertainty when using film as a detector can be defined by examining radiographic film's characteristics. One such area, which is often defined in literature on the subject, is film's lower energy photon over-response characteristic.[19,36,39-43] Film's increased relative sensitivity for low energy photons may be owing to the differences in attenuation between water and the active component of radiographic film – AgBr. Childress and Rosen (2004)[44] suggested, "*silver halide content overresponds to low energy photons because of an increase in photoelectric effect interactions*." Heydarian et al. (1996)[45] share the same notion in saying silver bromide, "*overrespond to the lower-energy and to a lesser extent to the higher-energy (E ≥1.02 MeV) photon beams, as a result of the photoelectric and pair production effects, respectively*." The over response of film is largest when exposed at greater depths, say 10 cm, then normalised to shallower depths, say 1.5 cm. This may be attributed to the change in the photon spectrum[19,36,43,46-50] and the absorption properties[19,24,45,47,51] of radiographic film. What this means is that the optical density (OD) of a film exposed with 100 cGy at the surface of a phantom will be different to the OD of a film if it was exposed with 100 cGy at a depth of 10 cm. Consequently, the relationship

[j] AGFA G334i two part universal fixer

between dose and OD would require redefinition if the film was exposed at various depths within the phantom.

Several practical problems arise when using radiographic film,[6,12,18,52,53] which include:

- The light absorption contributed by film's supportive layer (Base) may cause a systematic overestimate of the dose,
- The increase of optical density caused by the processing stage (Fog) may also cause a systematic overestimate of the dose,
- The precision of the sensitive layer may vary between batches manufactured at different dates, which may be a significant source of random error in measuring dose,
- The relative over response of film to dose with deeper phantom depths reduces the accuracy of depth dose measurements,
- Film processing: chemical control, washing and drying, darkroom control, processing time and temperature control.

The first disadvantage is an artefact of film manufacture and was investigated by analysing the variation of Base between film batches and subtracting the artificial film dose caused by the discoloration of Base. Fog was analysed together with Base (Base plus Fog) for convenience. Film's over response to lower energy photons is inherent with the use of silver halide film, but in this particular application it could be avoided by always measuring optical density at a single depth.

Two other potential problems may arise when using radiographic film to evaluate IMRT fields: film's dependence on multiple exposures (fraction dependence) e.g. is the dose measured for 1 × 50 cGy the same as the dose measured for 2 × 25 cGy? The second problem is exposure rate or dose rate dependence i.e. is there a difference in the response of the film for different exposure rates? Fraction dependence occurs during an IMRT field where areas exposed by radiation can be blocked, as the MLC moves into different positions, only to be exposed again with subsequent MLC motion. In addition, exposure rates are also altered to allow time for the MLC to move into position and consequently exposure rate (dose rate) effects were also examined.

2.7 *Film digitising.*

Digitising is a form of transforming an analogue image into digital form. Digitising film makes it possible to analyse and compare film images, and therefore measured data, with data calculated by a treatment planning system.

During film digitising, light from an extended source (I_0) is partially absorbed in film, on its way to a light-recording device (receiver, I). Darkened areas of a film passing through the digitiser, attenuate the initial light (I_0) reducing its intensity (I) at the receiver. Beer's law was formulated to describe the attenuating consequence of homogeneously distributed silver crystals on parallel beams of light traversing a film manufactured to have a uniformly thick active layer. Beer's law applies in the circumstance where the light beam has a spectrum with near uniform attenuation by the silver crystals and insufficient energy to affect the crystals in any way and in a measurement geometry that minimises the effect of any scatter resulting from light attenuation. Beer's law predicts that from the amount of light reaching the detector, it is possible to determine the optical density (OD), which for low doses is proportional to the dose given to the film.[54] In literature this is commonly referred to as OD, Niroomand-Rad et al. (1998)[21] refer to this as Absorbance (A) and it is defined as the logarithm of the fraction of light intensity (I_0/I) reaching the receiver. This is mathematically represented in equation 4. A logarithmic scale is used because Beer's law predicts a logarithmic response.

$$OD = \log_{10}\left(\frac{I_0}{I}\right) \qquad [4]$$

Some digitisers can digitise films in 8-bit or 16-bit shades of grey (greyscale or resolution). Greyscale represents the available fractions comprising the digitised image. For 8-bit, there are 2^8 available shades of grey. For monochromatic images, this amounts to 256 mutually exclusive shades between and including no saturation (white) and maximum saturation (black). The Vidar digitiser[k] used in this study can digitise film into monochromatic digital images up to 2^{16} (65536) fractions.

Several uncertainties can be identified when using digitisers to convert images.[18,55] One such uncertainty arises when digitising to 8-bit images,[18] which will reduce accuracy of converted images.

[k] Vidar VXR-16 DosimetryPRO digitiser

Distances can be distorted[55] resulting in incorrect displacements and OD measurements made inaccurate because of non uniform light sources.[l] For these reasons, the digitiser's light source was analysed for spatial output variation (uniformity), constancy over time (constancy) and accuracy at digitising distances (geometric accuracy).

2.8 Acceptance criteria.

The evaluation of simulated treatment plans involves comparing differences in images created from the treatment planning system (TPS), computed, and the linear accelerator (linac) using film, measured. These images are overlaid and evaluated for congruence.

When two similar images are placed over each other so that they match the images are correlated. For this study, digital field images created from film exposed on the linac were correlated with simulated field images created by the TPS. An evaluation of how well these images correlate, in terms of pixel magnitude changes and pixel displacements, is made against what are called acceptance criteria. A program called DoseLab was used to evaluate image correlation based on two acceptance criteria – dose differences (DD) and distance measurements to points of equal intensity (distance-to-agreement, DTA). The acceptance criteria are explained later. There are two conflicting reasons why acceptance criteria are used. Firstly, there is a limit to the achievable congruence between a computer generated model of what a linac will deliver, and a measurement of what is actually delivered, dictated by the precision and accuracy of the equipment used for this determination.[6] Secondly, there is threshold of accuracy required to achieve a curative and beneficial outcome for the patient.[56] From this it is clear that if the measurement equipment is not accurate enough, it will not be possible to determine whether the proposed treatment meets the requirements to achieve a curative and beneficial outcome. To consider this further, the details of acceptance criteria must first be reviewed.

Incorporating Mathworks MATLAB[m] functioning, DoseLab is able to calculate differences in correlated images using acceptance criteria. To register or correlate two images DoseLab uses the NORMXCORR2 MATLAB function. The MATLAB function compares two overlaid matrixes to find minimum correlation numbers. The function does not consider rotational orientations and consequently is limited to evaluating pre-registered images that match in rotation.

[l] N. Childress, M. S. Ron Vantreese and I. Rosen, DoseLab 3.05 User Manual, http://doselab.sf.net/ (2003)
[m] MATLAB, MathWorks Inc, Natick, Massachusetts, USA

To evaluate correlated images the developers of DoseLab created a method to support their idea of what should be acceptable. The method uses Boolean-type logic, which is illustrated in figure 5.

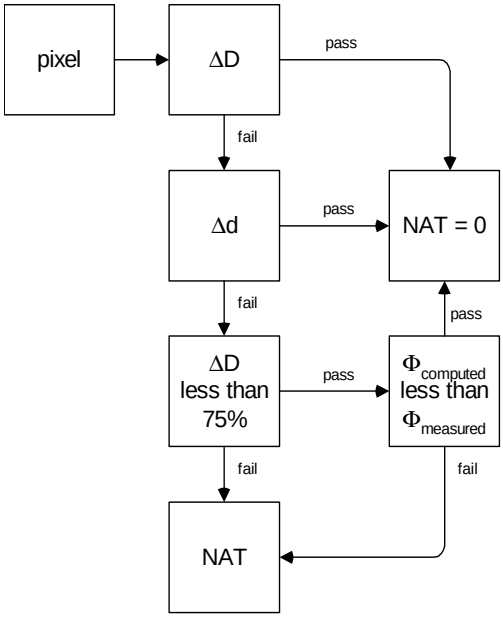

Figure 5. Illustration of the procedure used by DoseLab's NAT value in an image correlation evaluation. ΔD denotes the user's limit for dose difference (DD), Δd is the user's limit for distance-to-agreement (DTA), NAT refers to the normalised agreement test and Φ denotes the fluence generated by either the TPS (computed) or from the linac (measured).

The method depicted in figure 5 leads to the normalised agreement test (NAT) if all other alternatives are exhausted. This is similar in theory to already established acceptance criteria.[6,7,27,39,41,57-61] The NAT value is a measure of two criteria evaluated separately. The test first measures pixel magnitude variations (ΔD) and secondly distances (Δd) to the nearest pixel of similar magnitude. The acceptance criteria limits (*m*) for ΔD and Δd are customisable. DoseLab calculates a NAT value for each pixel in the correlated image. The developers[27] give the following reasoning for calculating the NAT value, "*the method of calculating NAT values ensures that a point falling within the ΔD_m or Δd_m criterion is not penalized or rewarded for being within systematic tolerances*."

Film dosimetry acceptance criteria are explained in more detail. The most reasonable criterion measures the magnitude difference between calculated (computed) and measured images. Known as the difference in percent dose or dose difference (DD or ΔD) it is a measure between pixel magnitudes in overlapping (correlated) images. The second criterion is a distance measure. It assesses the closest point in one image that has a similar pixel magnitude in the other image. This is known as distance-to-agreement (DTA or Δd) and is measured in millimetres. DTA was established for dose evaluations in regions containing steep gradients. Figure 6 illustrates use of the DTA. From figure 6, if DD were evaluated a large discrepancy would result within the steep dose gradient region. In this circumstance, an inappropriate rejection is made, because each profile is identical only one is displaced by two millimetres.

Childress and Rosen (2003)[27] shed more light on the evaluation or misuse of the DD contesting that, "*percent differences can easily become very large in low-dose areas, because they are divided by small numbers*." Likewise, it is less significant to have small monitor unit differences on fields that contribute to large percent errors although only add up to give, for instance, 50 cGy on a treatment that may have as many as 7000 cGy. This is less than 1% of the total dose and within international tolerance levels.[62]

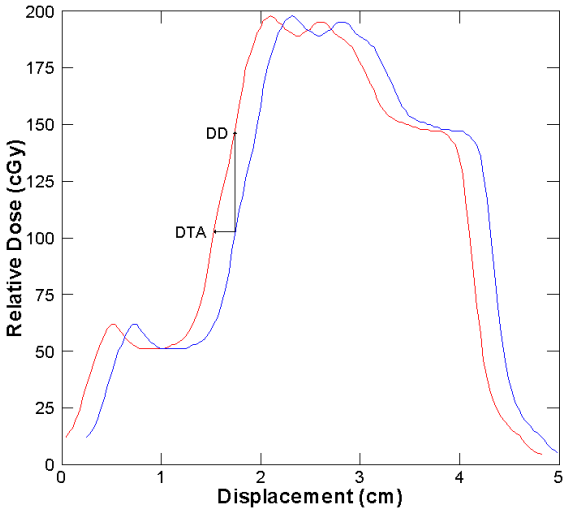

Figure 6. Profiles of a single IMRT field repeated with a 2 mm displacement. DTA refers to distance-to-agreement and DD refers to dose difference.

Deciding on the DD and DTA limits requires knowledge of the uncertainties inherent in film dosimetry. In an earlier publication, Van Dyk et al. (1993)[23] gave acceptance criteria for photon field dose

calculations in different regions such as central ray data, high dose gradients in low dose regions and low dose gradients in high dose regions.

What tolerance level should be used? Depuydt et al. (2001)[39] performed 3.3% and 3 mm tolerances for ΔD_m and Δd_m although they recognised, "*particularly large deviations, exceeding tolerance levels of ΔD_m = 5% and Δd_m = 4.5 mm*" for their prostate treatment fields using an electronic portal imaging device. Kapulsky et al. (2004)[7] accept dose differences of 5% stating, "*dose-difference values greater than ±3% among analyzed hybrid plans was 8.6% ± 3%.*" Among other statistics in the same article, "*dose differences greater than ± 5% was 1.7% ± 1%*" and, "*the number of pixels with more than ± 10% dose difference was negligible.*" Other authors[8,58-60] use limits of 3% and/or 3 mm. Winkler et al. (2005)[6] accept limits of 5% and 3 mm with uncertainties of 1.9% and 0.8 mm attributed to their IMRT film QA. Low and Dempsey (2003)[61] state they, "*typically use 5% and 2-3 mm in clinical evaluations.*" Childress and Rosen (2003)[27] accept limits for of 3% and 3 mm although their method of using these limits differ from the combined evaluation of the Gamma,[8,41,57,59] which evaluates the quadratic ratio for each criterion.

Childress and Rosen (2003)[27] give reasoning behind the differences between acceptance criteria in saying, "*because 2D quantitative comparisons of IMRT plans are not yet commonplace, it is difficult to recommend or set definite criteria for them.*" In this study, tolerance levels were restricted by equipment and method uncertainty.

2.9 The need for independent QA of radiographic film dosimetry.

Radiographic film dosimetry has several identified problems including depth and energy dependence[36] where the key ingredient in film responsible for image formation, silver-bromide, over responds to lower energy photons (about 400 keV). This over response overestimates the dose at greater depths where the ratio of lower energy photons to higher energy photons is greater. Yeo et al. (1997)[36] measured errors of 30% or more using film at depths greater than 20 cm. The energy dependence can also be related to field size[11] where changes in scattered radiation created by changing the field defining shielding blocks (Jaws) causes a mismatch response in film. This can cause errors of 65%[43] going from a 6 cm × 6 cm field size to a 25 cm × 25 cm field size. Depending on the orientation of the film, parallel or perpendicular to the field, orientation dependence[8] can occur. Bucciolini et al. (2004)[8]

measured the uncertainty for both orientations and found that the perpendicular arrangement yielded better with an uncertainty of 2.6% whereas the parallel method produced 3.4%.

Film developing[44] errors are also common; variations in optical density can occur between films processed on the same day (intra session) and processed on different days (inter session). This can cause uncertainties between 6.6%[12] and 15%[8] respectively. Converting the film into a digital form or digitisation can produce spatial distortions[55] when converting linear dimensions. Holmes and McCullough (1983)[55] found it reasonable to expect errors of 1 mm or 1% on measurements of length. There also exists the inability of planning computers to accurately model variations in the manufacture of multileaf collimators (MLC).[39] The MLC causes complex and varying penumbras, and variable transmission patterns. Depuydt et al. (2001)[39] found their treatment planning system applies a single 2% correction to compensate for the MLC leakage however their measured data showed a variation from 1.5 to 2.2%.

Table 1 demonstrates the film response variability by listing some of the results obtained from other authors. The table illustrates the variation between authors and thus the complexity arising when using radiographic film as dosimeter. For example, Ju et al. (2002)[14] measured a 15% error for film in a 6 MV beam (15cm square field) at 10 cm depth whereas Olch et al. (2002)[12] measured an approximate error of 2% for the same beam arrangement. Subsequently, this variation also illustrates the need for each centre to characterise the magnitude of these problems and apply them for their QA at their centre. The comparisons are primarily with ionisation chambers though software is also considered.

Table 1. Published film uncertainties in radiotherapy beams.

Author	*Exposure range*	*Max. error (%) or mm where specified*	*Mean error (%)*	*Photon beam at max. error (MV)*	*Depth of max. error (cm)*	*Field diameter of max. error*	*Intra session error (%)*	*Inter session error (%)*	*Film phantom material*	*Comparison for max. error (IC, film, TPS)*
Anderson & St. George (1979)[63]		5		25	>15	15			Polyisoprene	Ion chamber
[n]Bucciolini et al. (2004)[8]	10 - 140 cGy	3 or 3 mm		6		MLC	1	15	PMMA, solid water	Focus
[n]Bucciolini et al. (2004)[8]	<50 cGy	2.1		6		3, 5, 10, 20	1	15	PMMA, solid water	Varies
Burch et al. (1997)[43]	5 - 90 MU	65		4	30	25			Polystyrene	IC-10/Markus
[n]Burch et al. (1997)[43]	5 - 90 MU	4.5		4		6, 25			Polystyrene	IC-10/Markus
Butson et al. (2004)[64]	0 - 60 cGy	3		6	0	10, 20			Solid water	Attix 449
[o]Cadman (1998)[65]	50 cGy	7.8		C-60	21	10			Polystyrene	PS-033
Danciu et al. (2001)[15]	20 - 200 cGy	4		C-60	10	15	1	5	Wood	Film
Dogan et al. (2002)[11]	80 & 300 cGy	7.5		C-60	25	24	0.5	1.5	Polystyrene	Ion chamber
Esthappan et al. (2002)[66]	5 - 100 cGy	<4.5		6, 18	<15	<15			Water-equivalent	Ion chamber
Gotoh et al. (1996)[67]		4	1.4	10	20	21.5			Solid water	FDC-9.4UC
Hale et al. (1994)[68]	0.8 OD	16		C-60	0.5, 12	10			Polystyrene	Film
Ju et al. (2002)[14]	0 - 50 MU	15		6	10	15			Water	Multidata 9732
[n]Ju et al. (2002)[14]	0 - 50 MU	3		6	10	15			Water	Multidata 9732
Lewis et al. (2000)[69]	65 MU	47		4	0.1	12			Wood	Pencil beam
Mayer et al. (1997)[70]	<25 cGy	<5		15	15	10			Various	Ion chamber
Mayer et al. (1997)[70]	<25 cGy	12.9	7.0	4		20			Cork	ROCS TPS
Olch (2002)[12]	0 - 100 cGy	10		6	20	2	6.6		Solid water	PTW N30001
Olch (2002)[12]	0 - 100 cGy	14.3 or 4.48 mm		6		MLC	6.6		Solid water	Plato
[p]Paptheodorou et al. (2000)[30]	0 - 70 MU	5 or 3 mm		6	5	MLC			Polystyrene	ISiS3D TPS
Robar and Clark (1999)[19]	5 - 385 cGy	15		6	20	20	1.1	2.9	Solis water	Film
Stern et al. (2004)[26]		6.3 or 2 mm	4	18	10	4			Water-equivalent	Ion chamber
Stern et al. (1992)[22]	5 – 120 cGy	2.3 or 2 mm	1	15	20	10			Water-equivalent	IC-10/film
Suchowerska et al. (1999)[48]	10 - 80 cGy	62.4	24.7	C-60	25				Solis water	RK
Tsai et al. (1998)[29]	120 cGy	0.3		6	15	10			Polystyrene	Film
Tsai et al. (1998)[29]	55 cGy	4	1.9	6	14	10			Polystyrene	Ion chamber
van Battum & Heijmen (1995)[71]	50 cGy	1.3	<1	23	20	20	0.7	1.3	Water	Ion chamber
Wang et al. (1996)[60]	0 - 50 cGy	10		6	5	MLC			Polystyrene	MSKCC TPS
Williamson et al. (1981)[72]	10 - 350 cGy	3.1	1.2	4	17	5			Polystyrene	Ion chamber
Winkler et al. (2005)[6]	0 - 90 cGy	1.6		6	9	10	1.3		PMMA	Ion chamber
Winkler et al. (2005)[6]	0 - 90 cGy	1.9 or 0.8 mm		6			1.3		PMMA	Pinnacle
Yeo et al. (1997)[36]		~33		4	20	25			Solid water	Ion chamber
Zhu et al. (2002)[73]		2.5	0.9	23	20	5			Solid water	TN23343

Intra session refers to OD errors in films exposed and developed on the same day. *Inter session* refers to films exposed on one day and processed on another.
MU refers to a set dose unit on the linear accelerator and for a specific field arrangement and under specific circumstances, 1 MU is equivalent to 1 cGy.

[n] Filtration method, created by placing a thin metal sheet in the field that absorbs lower energy photons.
[o] CEA TVS radiographic film
[p] AFGA Structurix radiographic film

3 Equipment.

The following are basic characteristics of the apparatus used in this study. For some devices, certain concepts or functions were addressed in the background section to point out key features or limitations with the device and thus were omitted from this section.

3.1 AGFA model Curix HT-330 film processor.

Specifications for the AGFA Curix HT-330U are given in table 2. More information regarding on how the processor functions and what active ingredients are used are given in section 2.6. The processor resides by itself in a small room accessible only by a revolving dark room door. The two-way door has a felt sealing strip between two cylinders of which one rotates within the other. Light in the room is provided by a safelight with a red filter to allow a low level of light that safely allows processing of light-sensitive films while providing enough brightness for the human eye to detect.

Table 2. Manufacturer specifications for the AGFA model HT-330U film processor.

design	*specification*
Developer temperature	25°C to 39°C
Developer temperature accuracy	± 0.3%
Fixer temperature	34°C
Maximum film length	20 m
Minimum film width	43.5 cm
Minimum film size	10 cm x 10 cm
Operating environment	10°C to 30°C at 30% to 80% relative humidity, non-condensing
pH	6.5 to 8
Throughput	60 seconds (320 films/hour) 90 seconds (210 films/hour) 120 seconds (160 films/hour)
Serial number	2161
Warm up time	15 minutes
Water consumption during processing	3 l/min
Weight	160 kg (full tanks)

3.2 DoseLab.

DoseLab is a multifunction software application that assists in aspects of film dosimetry. The program was developed by Nathan Childress, Ron Vantreese and Isaac Rosen to compare and quantitatively evaluate two digital images. One valuable process of DoseLab is its intrinsic ability to correct for irregular light source digitisers. A film's digital image is capable of light uniformity correction using comma separated values (CSV) files. These files contain information representative of the digitiser's light source.

DoseLab is also capable of converting optical densities to dose. The application uses two input files to create a CSV file containing the OD to dose conversion. The first input file is a digital image of a film containing up to eight separate exposures. These exposures represent a user's dose range. The second input CSV file contains one row of nine numbers indicative of the film's dose. DoseLab uses CSV files to reference film OD to create third order quadratic functions with OD a function of dose. The software is limited to nine points constrained to a certain orientation other than this the dose range may be customised.

3.3 ePin – An electronic fiducial utility.

ePin is a software package that allows markers to be embedded into digital images. It supports 32-bit images from many different sources including Pinnacle and is capable of converting file extensions into reduced byte depth images. ePin was designed at the University of Arkansas for the Medical Sciences department of Radiation Oncology. ePin was utilised to convert fluence image files from Pinnacle into reduced byte depth images usable by DoseLab.

3.4 ImageJ.

ImageJ is and image processing and analysis tool operating in the Java environment. It can calculate statistical information in various formats and generate geometrical transformations for many file and byte types.

3.5 Kodak X-Omat V Ready Pack radiographic film.

The properties of Kodak radiographic film was discussed in the previous chapter under section 2.5.

3.6 Nuclear Enterprises model 2571 and 2581 ionisation chambers.

The Nuclear Enterprises (NE) model 2571 ionisation chamber is also known as a Farmer or thimble-type chamber. The NE ionisation chamber consists of an inner electrode supported by a stem and surrounded by a thimble. The thimble on the 2571 model is made from graphite and the stem from aluminium while the 2581 models are made from water equivalent plastic (c-552). The stem terminates in a long length of low noise bi-axial cable. Like all thimble-type chambers, an outer electrode shell encases a guarded central electrode. The cavity between the two electrodes is termed the collecting volume. Atomic reactions from radiation produce ion pairs in the air within the

collecting volume. Ions interact with an electric potential applied across two electrodes and a resulting charge or ampere measured. The magnitude of the charge is proportional to the incident radiation and compared to a standard. Hence, the charge collected in the chamber can be converted into absorbed dose. Figure 7 illustrates the NE 2571 ionisation chamber.

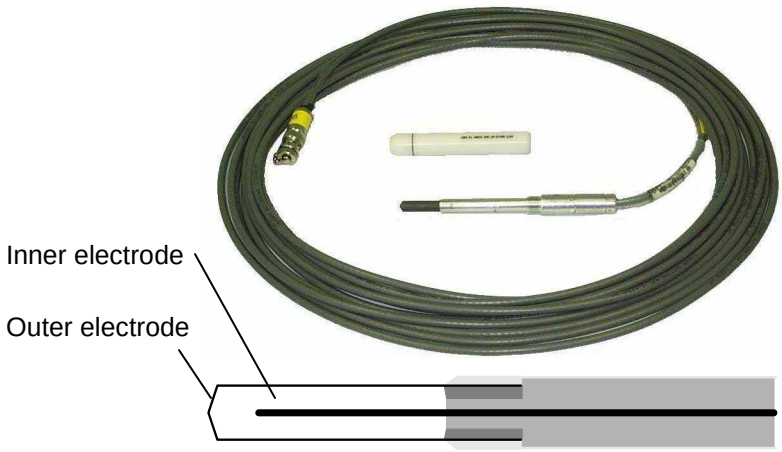

Figure 7. An image of a NE 2571 ionisation chamber with attached coiled cable and TNC connection. The white object above the chamber is a build-up cap used for C-60 in-air measurements. Pictured bottom is a schematically representation of the chamber adapted from Izewska and Rajan (2003).[74] The length of the chamber from top to tail is 13.7 cm however the length of the sensitive volume is 2.4 cm.

3.7 Philips Pinnacle treatment planning system.

Pinnacle (version 7.6) is a software application that is capable of simulating a series of radiotherapy linear accelerator parameters to create a plan for the delivery of a therapeutic dose. The purpose of the software is to provide support for people who are appropriate candidates for radiotherapy treatment and guide the course of a patient's treatment. The software is capable of calculating absorbed dose in a radiotherapy photon beam with 3D convolution superposition algorithms using data generated from computed tomography. It is composed of a UNIX workstation using the Solaris[q] operating system.

3.8 Polystyrene $(CH_2)_n$ phantom.

Polystyrene, or the close approximation Solid Water (SW), imitates the characteristics of water i.e. it has similar scattering and absorption properties of water. In external beam radiotherapy, it replaces water for convenience because it is solid at room temperature and can be handled with ease. When

[q] Sun Microsystems, Inc. Santa Clara, California, USA

cut to size, it makes for highly reproducible and quick setup times. SW is easily movable and opaque which gives it great versatility. The IAEA report[75] recommends, "*plastic phantoms can be used for routine quality assurance measurements, provided the relationship between dosimeter readings in plastic and water has been established for the user beam at the time of calibration*." SW was chosen as the phantom material for this investigation.

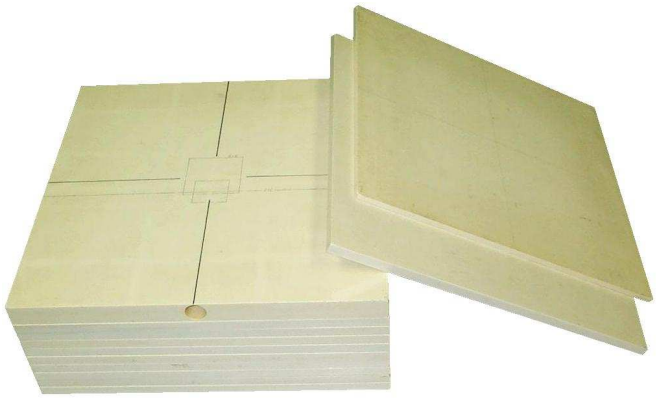

Figure 8. Photograph of the sectioned sheets of solid water. Sheets have dimensions of 1 cm × 30 cm × 30 cm. The topmost-stacked sheet is an ionisation chamber holder designed to hold the NE 2571 chamber. The holder is twice the thickness of regular sheets. Discoloration is from grit deposited from manual handling and radiation damage. New SW material appears an opaque white or brown.

3.9 Varian linear accelerators.

A linear accelerator is a device that produces electron and X-ray ionising radiation. It comprises of a wave-forming network, an electron gun, an accelerating guide and field defining structures. The wave-forming network produces microwaves in short bursts for the accelerating guide. The guide is manufactured to use microwaves to accelerate electrons to a few mega electron volts. The radiation produced is focused and shaped with thick tungsten blocks called secondary Jaws. On the centre's 21EX machine, a 120 leaf multileaf collimator is attached to create more conformal shapes. Figure 9 illustrates the Varian model 21EX linear accelerator.

Figure 9. A photograph of the Varian model 21EX linear accelerator. The beige-like section represents gantry orientation and rotates about a midline point 100 cm from a focused X-ray source, not viewable, and stands about 2.4 m in height. The present orientation of the gantry is zero degrees. The brown rectangular object at the base of the gantry is an electronic portal imaging device. A digital readout pictured in the centre of the gantry displays the current position of the collimator, gantry and Jaws. The dark stand positioned immediately behind the gantry houses some of the electronic components described in this section. The electron gun, accelerating guide, bending magnet, carousel and collimating devices are housed in the beige-like section that rotates when the gantry moves.

3.10 Vidar model VXR-16 DosimetryPRO digitiser.

The Vidar is a digitiser somewhat similar to a flatbed scanner only it is more accurate, more precise and has better resolution. Contained within the digitiser are a broadband ultraviolet light transmitter and a charged coupled device (CCD) receiver. The CCD is a matrix of photodiodes where the photodiode is a semiconductor. The matrix of photodiodes and the ultraviolet light form the transmitting and receiving components.

Figure 10 shows the Vidar model VXR-16 DosimetryPRO digitiser. The foot of the device is approximately 41 cm × 50 cm. Digitising requires positioning film on the top like a sheet of paper would be positioned for printing. During digitising the film is automatically driven between the transmitter and receiver components. As the film moves, the light source remains constant. Vidar specify a dimensional accuracy of better than 1% or 2 pixels whichever is greater for either dimension.

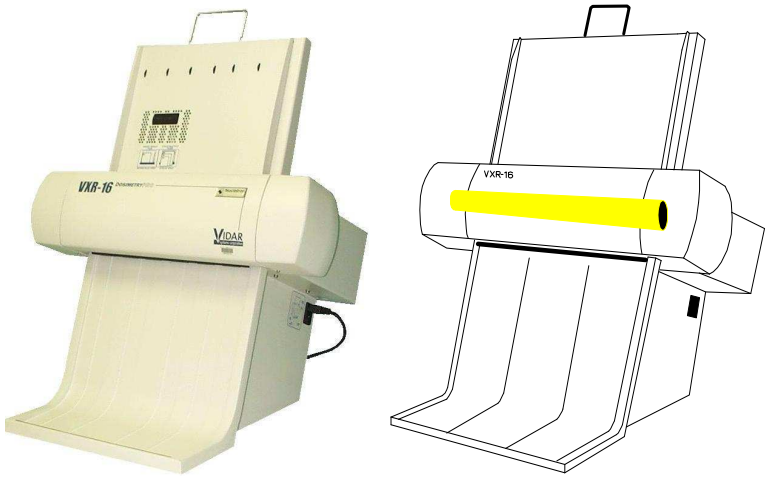

Figure 10. The left-hand side of the figure shows a photograph of the Vidar VXR-16 DosimetryPRO digitiser. The right-hand side of the figure gives an approximate location of the UV light source contained within the device, highlighted in yellow. At the top is the film holder and at the base a film trap. The device is approximately 82 cm in height.

Driving the film through the digitiser are small motors of variable speed. This is termed by Vidar as Exposure and ranges between 8 and 40. For the slowest velocity setting (Exposure 40), the digitiser drives the film through at about 1.8 cm/s. For the fastest speed setting (Exposure 8), it is about 4.4 cm/s. Increasing the speed of digitising allows darkening of the image and vice versa.

Film may be auto sized to suit individual films and a standard small film digital image (TIFF), 25.4 cm × 30.5 cm, for a 71.25 dpi is approximately 1209 kB. The image size extends to 34058 kB for 285 dpi in 16-bit. The digitiser is also capable of using several translation tables for converting light transmission. These tables include linear, optical density (OD) and custom for user-defined tables. Mersseman and De Wagter (1998)[35] describe the purpose of these tables saying that the linear translation table simply multiplies the transmission by a number and the OD translation table, "*transforms the pixel values logarithmically so that the resulting integer value is nearly proportional to the OD*."

3.11 Victoreen model densitometers.

The Victoreen digital densitometer is another form of digitiser. It is designed to measure optical density ranges below 4.5 OD. A white LED transmitter mounted on an arcing arm creates spectral radiance at approximately 465 nm. A transparency such as a film is placed between the transmitter and receiver. A silicon diode measures the resulting diffuse signal and displays a number representative of the OD. Figure 11 illustrates the Victoreen densitometer.

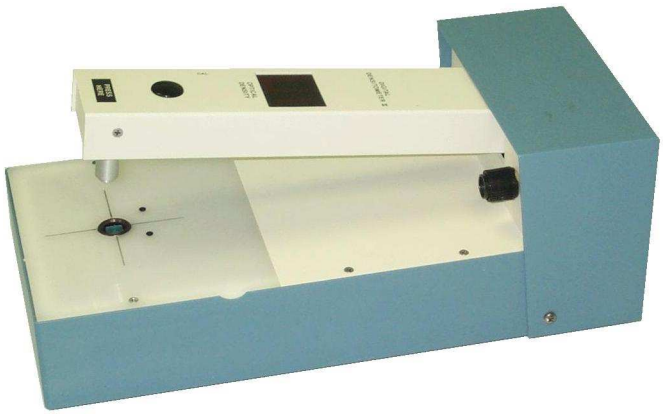

Figure 11. A photograph of the Victoreen densitometer showing a small angled pivot arm that contains the receiver and that is above an LED transmitter. Film is placed in gap between the arm and transmitter, the arm is pressed on the film and a reading is displayed on the arm. Image is for the model 07-424 densitometer. The foot of the device is 15.5 cm wide and 33.0 cm in length.

Two models of the Victoreen densitometer were used: models 07-424 and 07-443. Both densitometers have the same accuracy, range and detectors although the model 07-424 has a greater range.

3.12 Victoreen Keithley model 35040 electrometer.

The Keithley model 35040 electrometer is designed to measure charge or charge rate from an ionisation chamber. It is operated for diagnostic radiotherapy and conformal radiotherapy dosimetry. Capable of providing bias voltages between -500 V and +500 V with an accuracy of ±0.3 V for loads less than 0.2 mA. The user is able to input temperature, pressure, leakage limits and absolute dose constants. The front panel has a selectable display screen for dose, dose rate, effective exposure time, mean current or rate measure. For convenience, the electrometer has both front and rear triaxial network cable ports and an auto reset. Figure 12 illustrates the Victoreen model 35040 electrometer. For part of this study measurements were performed on another electrometer, Scanditronix-Wellhöfer model Dose1, because the Keithley was unavailable.

Figure 12. An image of the Keithley model 35040 electrometer. Various menus can be assessed through the front screen shown by the green illuminated panel. Access to the electrometer is obtained either through the front TNC port or at the rear of the device. The base of the device is approximately 50 cm × 50 cm.

4 Methods.

This chapter describes the method used to measure and correct for uncertainty in digitising, processing and characterising the response of radiographic film. The quality of the digitiser's light source and light receiving device was assessed. Tests included light output uniformity and constancy, as well as geometric accuracy. Film processing uncertainty was determined by delivering known doses to a number of films in a standard setup over several months, then comparing optical density differences. For characterisation of the radiographic film response, four characteristics were measured: Base plus Fog, dose rate dependence, dose fraction dependence, and variation between film batches (homogeneity). The chapter also describes the methods used to compare simulated patient fields from the treatment planning system with those calibrated from film measurements using DoseLab.

4.1 Digitiser characterisation.

To characterise the VIDAR VXR-16 digitiser three distinct components are required. Firstly, an evaluation must be made of the light uniformity across the digitiser. Secondly, the intensity of the light reaching the detector must be monitored for constancy over time. Finally, the components that direct a signal to the receiver must be assessed for geometric accuracy. Each of these is dealt with in turn in the following subsections.

4.1.1 Light source uniformity.

To ascertain the uniformity of the digitiser's light source a homogenous semi-opaque transparency of dimensions comparable to the width of the digitiser was utilised. In this document this is called a Uniform Standardisation Template (UST). The UST was created by stacking together three small Kodak X-Omat V radiographic films (25.4 cm × 30.5 cm). The films were processed with no exposure, which left behind the semi-opaque film base. Three films were needed to produce an optical density in the expected range for exposed films in IMRT verification.

Films were inserted into the digitiser in a left-most justified orientation to ensure reproducibility and adequate coverage of the light source. Figure 13 illustrates the orientation of the film during digitising and the direction of the profiles measured on the film (horizontal and vertical). Films were digitised using the Vidar VXR-16 TWAIN interface with the linear translation table (firmware version 7.24). Translation tables are used by the TWAIN interface to convert the raw transmission data into a greyscale image. For example, a translation table can be selected to convert the raw transmission

data to optical density by applying a logarithmic function. During this project, it was the raw transmission values that were of interest, since conversion to optical density is performed subsequently in the DoseLab software. Hence all films were digitised using the linear translation table, which results in raw transmission values without any correction. Images were saved as TIFF files. These files were imported into DoseLab and profiles generated. MS Office Excel[r] 2003 was utilised for statistical evaluation.

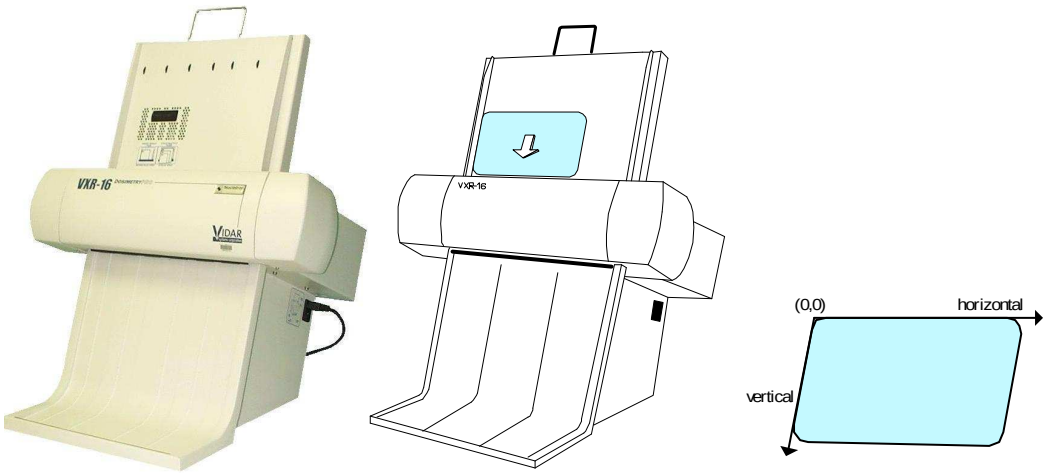

Figure 13. The method adopted for digitising the UST. This orientation encompasses the majority of the digitiser's width. Pictured right is an illustration of the profile direction for digitised images. Horizontal denotes profiles in the left to right direction (across the light source) and vertical denotes profiles orientated top to bottom (in the direction of film movement). These axes are recorded as displacement measures from the origin, (0, 0), which is the left-most and top-most position of the film.

Prior to each digitisation an internal calibration was performed, with the goal of placing the digitiser in a reproducible state. The VIDAR TWAIN User's Guide[s] states, "*Calibration directs the film digitizer to calibrate white and black levels. Calibration compensates for pixel to pixel variations in both the white and black ends of the grayscale to produce an even, consistent scan*." For each film, horizontal profiles at several locations were measured from a total of twenty digitisations of the UST. Profiles at displacements 3.6 cm (pixel 100), 12.5 cm (350) and 21.4 cm (600) from top to bottom were analysed.

[r] Microsoft Corporation, Redmond, Washington, USA
[s] Vidar Systems Corporation, VIDAR TWAIN User's Guide, www.vidar.com (2005)

The analysis was repeated for three different Exposure settings, which corresponded to the minimum (Exposure 8), optimum (12) and maximum (40) speed. Reiterating, the digitiser interface controls the speed of film movement through the digitiser by setting Exposure, which is the time in milliseconds for which light strikes the CCD array for each scan line. Possible Exposure settings are integer values between 8 and 40. Variations in signal along a horizontal profile can arise either from variations in optical density on the UST, or spatial variation in the light source intensity.

Vertical profiles were also analysed for each of twenty digitisations of the UST. Points on a vertical profile represent the transmission of a specific part of the light source as the film is driven through the digitiser past the stationary light source. Variations in signal can arise either from variation in the optical density on the UST or temporal variation in the light source intensity. For each film, profiles at 8.9 cm (pixel 250) and 23.2 cm (650) from left to right were analysed.

4.1.2 Light source constancy.

The method for measuring the constancy is similar to the method described for measuring uniformity (section 4.1.1) except three larger films (33 cm × 41 cm) were used to cover the full width of the digitiser. Digitisations of this UST were performed at intervals over a period of five months. Profiles from these digitisations were compared. Single horizontal profiles were measured using DoseLab at 18.4 cm (pixel 515). This area was chosen because it was the least altered by scratches created during repeated digitising (see section 5.1.1).

4.1.3 Geometric accuracy.

Displacement uncertainties from digitising were measured using a single film that contained lines and squares of known dimensions marked by a fine felt-tipped pen mounted on an X-Y plotter. This is called a Displacement Standardisation Template (DST). From DoseLab, horizontal and vertical profiles measurements of the DST, 1 cm either side of the centre, were created. An analysis incorporated three Exposure settings (Exposure 8, 12 and 40). The distance between peaks in each profile was compared to actual displacements on the DST as measured with a ruler.

4.2 Film processor characterisation.

To investigate the reproducibility of the AGFA Curix HT-330 film processor, OD-to-dose curves were measured on different days with the same batch of film. Differences in optical density from day to day are expected to be caused by differences in processing conditions (see section 2.6), but results

could also be influenced by film to film variation. Experiments were repeated using self developing radiochromic film to examine the uncertainties associated with measuring OD-to-dose curves by excluding processing uncertainties.

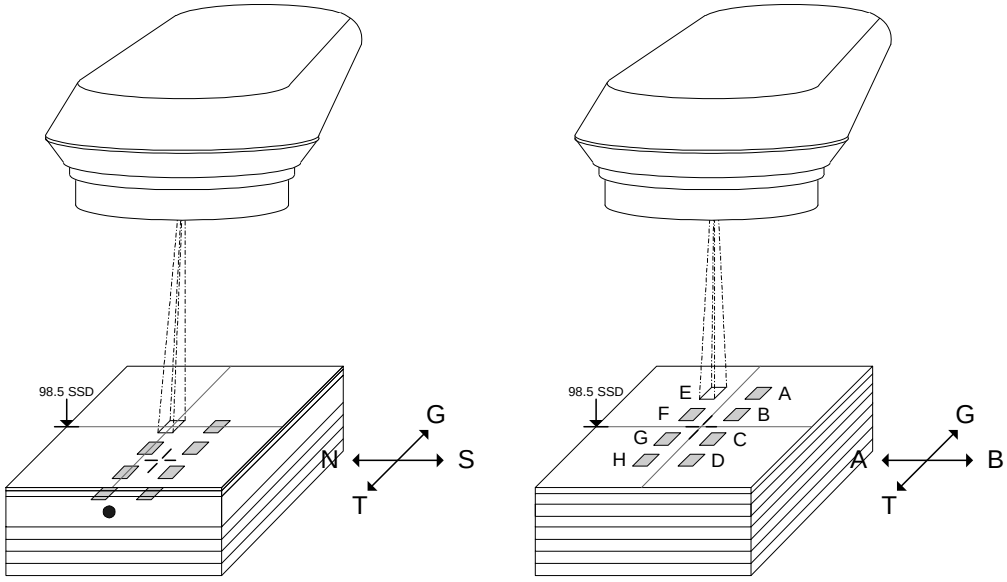

Ion chamber setup

Film setup

Figure 14. Illustration of the ion chamber and film arrangement used in the OD-to-dose procedure. For ion chamber measurements, each field is measured by moving the phantom and ion chamber to every location (pictured left). For film measurements, the phantom and film remain stationary as the Jaws are repositioned for each location.

The procedure for calibrating film was adapted from a method described by Childress and Rosen.[t] Each film was placed at the depth of dose maximum in a solid water phantom, and exposed to eight separate 5 cm × 5 cm fields, using an asymmetric setup. This is shown in figure 14 and tables 3 and 4. The linac was set to deliver between approximately 20 cGy to 190 cGy per field. Each field was allocated identification A – H in order of the magnitude of the dose delivered, as seen in table 4, and defined in this document as a measurement location e.g. location A. The same doses were delivered for both radiographic and radiochromic film, for consistency, although the radiochromic film requires a higher dose to achieve the same optical density.

[t] N. Childress, M. S. Ron Vantreese and I. Rosen, DoseLab 3.05 User Manual, http://doselab.sf.net/ (2003)

Table 3. Ion chamber and film arrangement in the OD-to-dose procedure.

Parameter	Ion chamber	Film
Collimator	0°	0°
Gantry	0°	0°
SSD	98.5 cm	98.5 cm
Depth to effective point of measurement	1.5 cm	1.5 cm
Solid water backscatter	10 cm	10 cm

Table4. Linac independent Jaw setting for the OD-to-dose procedure.

Location ID	A	B	C	D	H	G	F	E
Set dose (cGy)	20	40	60	80	190	160	130	100
Y1	-8	-1	6	13	13	6	-1	8
Y2	13	6	-1	-8	-8	-1	6	13
X1	7	7	7	7	-2	-2	-2	-2
X2	-2	-2	-2	-2	7	7	7	7

Radiographic film was processed using the automatic processor, set to 2 min and 34 °C. Prior to the processing of each film, five blank films were processed in an effort to ensure chemistry control.[1] The optical density of both the radiographic and radiochromic films was measured at nine separate locations on each film – at the centre of each of the eight fields (A-H), and at an extra location at the centre of all fields, designated O, to measure scattered radiation. Measurements for the radiographic film were done using the Victoreen model 07-424 densitometer and for the radiochromic films using the Victoreen model 07-443 densitometer. The model 07-424 was unavailable when the radiochromic film measurements were made. The specifications for the two different densitometers are shown in table 5. Both densitometers measure optical density at a single location on a film with similar accuracy and resolution, and can be considered equivalent for the purposes of this project.

Table 5. Manufacturer specifications for the Victoreen model densitometers.

Design	Specification	
	Model 07-424	Model 07-443
Accuracy	± 0.02 D	± 0.02 D
Density range	0 to 4.50 OD	0 to 4.00 OD
Detector	Silicon photodiode	Silicon photodiode
Detector light source	White LED	Ultra bright lamp
Display	3 digits	3 digits
Serial number	95601	5416

To determine the dose to the film, the setup was recreated using a Farmer type ionisation chamber – see figure 14. The ion chamber was successively positioned at each of the nine measurement locations. At each location, the electrometer reading was recorded separately from each of the eight fields, and summed to give the total reading. A typical set of readings at one location (E) is shown in table 6. As seen in table 6, the total at each location includes the scatter from all the other fields. Readings were corrected for influence quantities and absolute dose calculated according to the recommendations in the IAEA's TRS 398.[75]

Table 6. Typical set of ion chamber readings at one location (E) in the OD-to-dose procedure.

Set dose (cGy)	20	40	60	80	100	130	160	190
Readings (nC)	0.02020	0.01990	0.01855	0.01585	21.63	0.39760	0.14362	0.13876
	0.02033	0.01989	0.01854	0.01587	21.62	0.39780	0.14356	0.13888
	0.02035	0.01988	0.01852	0.01583	21.62	0.39770	0.14362	0.13884
Mean (nC)	0.02029	0.01989	0.01854	0.01585	21.623	0.39770	0.14360	0.13883
Dose (cGy)	0.093	0.091	0.085	0.073	99.326	1.827	0.660	0.638
Total dose of all contributing fields at location E								102.793

For the radiographic film experiments, a Farmer model 2571 chamber was used with a Keithley model 35040 electrometer. For the radiochromic film experiments, a Farmer model 2581 was used with Scanditronix-Wellhöfer model Dose1 electrometer, since the 2571 was not available. The difference in dosimetry systems is not considered to be significant since both chambers had absolute calibration factors traceable to ARPANSA,[u] both have similar collecting volumes and hence a similar sensitivity, and both systems are suitable for measuring dose accurately.[75]

The optical density from the film was plotted against the dose determined by the ion chamber to produce an OD-to-dose curve. Experiments were repeated on 10 separate days.

4.3 Radiographic film characterisation.

For characterisation of the radiographic film response, four characteristics were measured: Base plus Fog, dose rate dependence, dose fraction dependence, and variation between film batches (homogeneity). Base plus Fog was measured from the transmission through an unexposed radiographic film relative to full transmission. Dose rate dependence was measured by exposing film to the same dose but at different dose rates as determined by the linear accelerator. Dose fraction dependence was measured by exposing film to the same total dose in either one, two or three

[u] Australian Radiation Protection and Nuclear Safety Agency, Yallambie, Victoria, Australia.

fractions. Film homogeneity was measured by comparing Base plus Fog values from two different film manufacturing batches. Methods for determining each of these characteristics are described in turn in the following subsections.

4.3.1 Base plus Fog.

Base was removed using a two-step process. The first step was to make use of the digitiser's Exposure setting. A single clear film was digitised for each Exposure setting and the maximum transmission, $T_{\max}$, recorded. The purpose of this test was to find the optimal Exposure setting that would measure close to 100% transmission even with the film's Base present and without saturation. The Exposure setting was incrementally increased until transmission was maximised. Exposure 12 was found to be the optimum setting while Exposure 13 was found to cause saturation.

The second step makes use of the DoseLab process for correcting uniformity. According to the DoseLab manual, the uniformity correction is based on a single profile, obtained by scanning a single unexposed film using the linear translation table of the digitiser. The software divides the transmission in the correction file by the transmission of the newly scanned image for each row of data and takes the log of the ratio to calculate optical density. The OD is multiplied by a factor of 20 000 to make integer values for saving as a 16 bit TIFF file. The calculation is expressed in equation 5.

$$OD(x) \times 20000 = 20000 \times \log_{10}\left(\frac{T_{corr}(x)}{T_{image}(x)}\right) \qquad [5]$$

Where: $OD(x)$ is the optical density at position x on the horizontal profile,

$T_{corr}(x)$ is the transmission from the correction file at position x, and

$T_{image}(x)$ is the transmission of the scanned image at position x.

As a result, when an area of the film is scanned where there is no dose, then the attenuation will be entirely due to Base. In this case, $T_{image}(x)$ will be equal to $T_{corr}(x)$ and the calculated optical density will be zero, as expected. In other words, using this procedure to correct for the Vidar's light source uniformity also corrects for Base.

In this project, the uniformity correction file for DoseLab was obtained by averaging the 60 profiles measured from the 20 digitisations of the UST, as described in section 4.1.1. Since the UST was composed of three films, the maximum transmission of the UST was significantly less than for a single film. If this was used directly as the uniformity correction file in DoseLab, this would result in negative optical densities when scanning background regions in single films, since T_{corr} would be less than T_{image} in equation 6. Accordingly, the uniformity correction file obtained from the three-ply UST was scaled to match the maximum transmission from the single film scanned at Exposure 12.

$$T_{corr}(x) = \left(\frac{T_{\max}^{\text{single}}}{T_{\max}^{UST}} \right) \times T_{UST}(x) \qquad [6]$$

Over the duration of the project, Fog was included in Base measurement because the measurement of Fog was regarded as impractical and beyond the scope of this research.

4.3.2 Dose rate dependence.

For film's dose rate dependence, dose rates of 200 cGy/min and 600 cGy/min were compared in a 6 MV photon field. Dose rates were chosen to represent actual dose rates of IMRT fields, which are modulated during delivery. Field setup parameters were: a field size of 10 cm × 10 cm, 100 cm source distance, 1.5 cm solid water build-up, and 10 cm solid water backscatter. Each film was exposed in succession, processed and digitised together. Films were processed at the same time to maintain consistent chemical concentrations or at least to limit the excessive depletion and recovery of active ingredients. The experiments were repeated on three separate days to assess the reproducibility of the results.

The mean transmission within a region of interest on each film was measured using ImageJ.[v] ImageJ was the preferred analysis tool chosen for measurements because of its functionality in producing region of interest statistics and for its ease of use. Figure 15 shows the location of the region of interest. Average transmission was calculated for the region, which consisted of 116 × 116 pixels at 71.25 dpi.

[v] National Institute of Mental Health, Bethesda, Maryland, USA

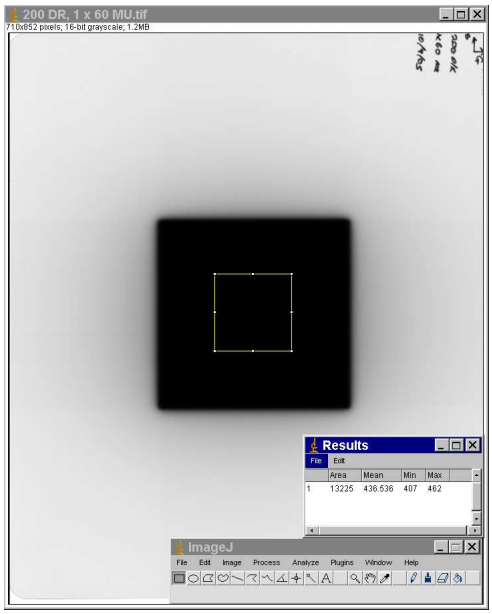

Figure 15. An image of the analysis tool from ImageJ used to measure an area of an exposed and processed Kodak X-Omat V film. Pictured centre is the exposed part of the film (black). Centred in the exposed area is the region of interest (yellow). The active window (bottom) displays region of interest statistics.

Measurements with a Farmer model 2571 ion chamber were performed using the same setup for comparison.

4.3.3 Dose fraction dependence.

The method for determining film's fraction dependence is similar to the method described in section 4.3.2. Three sets of three films were exposed with 60 cGy using different fractionations. The fractions included 1×60 cGy, 2×30 cGy and 3×20 cGy with 200 cGy/min and 600 cGy/min dose rates. A 6 MV photon beam was used on a solid water phantom with the film placed at 100 cm source distance, 1.5 cm build-up and 10 cm backscatter. Films were processed and analysed using the methods described in section 4.3.2. Measurements with a Farmer model 2571 ion chamber were performed using the same setup for comparison.

4.3.4 Film homogeneity.

The uncertainty arising from variations in film manufacturing was determined by measuring horizontal profiles. The Base plus Fog of two films from two different production batches was measured using a similar method as described in section 4.1.1 however a single film was used for both batches. These films were unexposed and processed then digitised using Exposure 12. The light

source uniformity correction from section 4.3.1 was not applied and a single profile centrally located was measured in DoseLab.

4.3.5 Radiographic film energy sensitivity dependence.

Several authors[19,36,41,43] advise radiographic film over estimates the dose corresponding to energies below 400 keV. Burch et al. (1997)[43] state, "*the problem occurs because of the presence of photons with energies below 400 keV for which the photoelectric effect is significant.*" Information provided by Johns and Cunningham (1983)[76] suggests this energy is below 25 keV for photon interactions with water. Stern et al. (2004)[26] state, "*film response increases at energies below approximately 300 keV*" a magnitude also stated by Esthappan et al. (2002).[66] The authors[66] state this may increase the film's sensitivity, "*caused by dominance of photoelectric interactions due to the film's silver content.*" Niroomand-Rad et al. (1998)[21] suggest that radiographic film has a large uncertainty in evaluating photon energies between 10 to 200 keV. Cadman (1998)[65] believed this energy is, "*below about 200 keV.*" Film's increased relative sensitivity for low energies may be owing to the differences in attenuation between water and the active component of radiographic film - AgBr. Childress and Rosen (2004)[44] suggested, "*silver halide content overresponds to low energy photons because of an increase in photoelectric effect interactions.*" Palm et al. (2004)[46] added that it is the, "*ratio of mass-energy absorption coefficients for photographic film to water*" that varies with energy and makes radiographic film over respond. Robar and Clark (1999)[19] suggest photons are preferentially absorbed by the emulsion owing to the Z_3 dependence of the photoelectric cross section. Krane (1988)[77] suggests, "*the probability for photoelectric absorption is difficult to calculate*" however from experimental studies, "*it is most significant for low-energy photons (~100 keV), it increases rapidly with the atomic number Z of the absorber atoms (roughly as Z_4), and it decreases rapidly with increasing photon energy (roughly as E_γ^{-3}).*" Robar and Clark (1999)[19] suggest that the linear attenuation for the emulsion increases at approximately E^{-3}. Film over response may in fact be a result from the photoelectric absorption for Ag or Br or more specifically from the difference in cross section around K-electron binding energies from water to silver.

Wang et al. (2002)[78] suggest, "*K-shell binding energy is 25.5keV*" for silver atoms of atomic number 47 and for tissue substitute materials such as gelatin it is 0.5 keV. They bring more evidence into the debate saying causes of, "*background densities*" around the tail of profiles is from Auger electrons and characteristic X-rays, "*created in the film, not the phantom*." The K-electron binding energy may be responsible for the increase in cross section which results in the over response for radiographic film. Lewis et al. (2000)[68] state, "*the relatively high sensitivity at low photon energies (especially near*

the silver K-edge, 25 kV) complicates evaluation of photon beams having significant low-energy contributions to the spectrum."

Heydarian et al. (1996)[45] share the same notion in saying silver bromide, "*overrespond to the lower-energy and to a lesser extent to the higher-energy (E ≥ 1.02 MeV) photon beams, as a result of the photoelectric and pair production effects, respectively.*" Some interesting results gathered by Danciu et al. (2001)[15] for AGFA Structurix D2 radiographic film showed sensitometric linearity up to 0.8 optical density for this dual-layered cubic grain silver halide emulsion film. This relationship is identical to radiochromic film which is excluded from the over response. By taking electron micrographs of Kodak X-Omat V film, Cheng and Das (1996)[37] showed the variation of grain to be marginally different, "*with the largest more than 10 times bigger than the smallest.*" Danciu et al. (2001)[15] refer to the AGFA film as having, "*cubic grain distribution*" which may be the underlining characteristic associated with radiographic film's over response. Bird et al. (1969)[42] add more to the debate by saying, "*typically, a dissolved sensitizing dye is added to the suspension of crystalline AgBr, and the active dye is found to be absorbed (usually chemisorbed) to the surface of the crystal.*" Hence, "*sensitizing dyes act as action transfer agents for absorbed photons of long wavelength*" i.e. lower energy photons. Silver bromide is a constituent of silver halide which also contains iodine though the purpose of the iodine is unknown.

Kodak X-Omat V film's over response may be due to the iodine component rather than all of the above-mentioned reasons. This may give evidence to why AGFA Structurix D2, which is comprised of silver bromide, has very similar characteristics to radiochromic film. Reasoning rests with the mass attenuation coefficient however other alternatives have to be explored to clarify any argument made. Dyes, crystal size and shape may play just an important role in silver halide over response. This is, however unfortunate, all inconsequential since it stretches beyond the scope of this research.

4.4 Error analysis.

Where applicable, results are given using the Coefficient of Variation (CoV). The CoV is a measure of the distribution (σ) normalised to the mean ($\overline{\mu}$) and is described by equation 8.

The mean is given by:

$$\bar{\mu} = \frac{1}{n}\sum_{i=1}^{n} X_i \qquad [7]$$

Hence the CoV is:

$$CoV = \frac{1}{\bar{\mu}}\left[\sum_{i-1}^{n}\frac{\left(X_i - \bar{\mu}\right)^2}{n-1}\right]^{\frac{1}{2}} \qquad [8]$$

4.4.1 Film dosimetric uncertainty.

As discussed in section 2.8, the overall uncertainty in film dosimetry is required in order to define an acceptance tolerance for the dose difference in the NAT analysis. To determine the overall uncertainty, the error associated with each section was considered separately.

Light source uniformity was corrected for using the method described in section 4.1.1. The errors associated with the light source uniformity and Base plus Fog were assessed using this method. Light source constancy was derived from the coefficient of variation for the five-month evaluation of the light source constancy (section 4.1.2). Geometric accuracy is considered in the distance to agreement part of the NAT analysis and does not contribute to dose uncertainty and therefore dealt a separate section (section 4.4.4).

To assess the impact of film processing on the NAT analysis the shape of the OD-to-dose curve was assessed for consistency. Specifically, a single film was converted from optical density to dose using two different OD-to-dose calibration files. The two calibration files were chosen from those obtained using the methods described in section 4.2, and had the minimum and maximum OD values for a given delivered dose. The reasoning for this is explained in section 5.5. These two resulting dose images were compared in DoseLab. For NAT analysis, it is the relative uncertainty that is of significance so that an error of 2 cGy out of 200 cGy is as important as 1 out of 100. For this reason, dose differences were determined for specific bins and an absolute average calculated over all bins. A full discussion on the derivation of film processing uncertainty is presented in section 5.5.

The error in Base plus fog is included in the error determination of the light source uniformity as outlined above and does not need to be determined separately. The uncertainties for the dose rate dependence and the dose fraction dependence were considered although not included in the final film dosimetry error. This is explained in sections 5.3.2 and 5.3.3. Film homogeneity was determined by comparing the Base plus Fog of different film batches.

4.4.2 Linac dosimetric uncertainty.

Variations in linear accelerator output from day to day do not contribute to the uncertainty in NAT analysis, since films are normalised to the planning computer fluence map prior to analysis. A variation of dose across the field from beam steering (symmetry) was taken from local tolerances.

4.4.3 Overall dosimetric uncertainty.

The total dosimetric uncertainty was calculated by summing in quadrature all contributions from sections 4.4.1 and 4.4.2 as shown in equation 9.

$$total = \left[(\text{" } film\text{"})^2 + (\text{" } processor\text{"})^2 + (\text{" } digitiser\text{"})^2 + (\text{" } linac\text{"})^2\right]^{\frac{1}{2}} \quad [9]$$

4.4.4 Geometric uncertainty.

There are three contributing factors to geometric uncertainty in the NAT analysis. The first is geometric accuracy, which is described in section 4.1.3 and fully discussed in section 5.1.3. The second is the uncertainty due to variations in MLC leaf movement during IMRT delivery and was taken from Sastre-Padro et al. (2008)[79] leaf positioning errors for the Varian Millenium MLC. The third is the accuracy of the process used to align the measured film with the computed field (fluence) in DoseLab as described in section 2.8. From the image pixel size of 0.356 mm, a standard error of 0.16 mm was assigned to the use of both the ePin and the pin prick, this being the radius of a circle that has 65% of the area of a pixel. These two were then summed in quadrature to obtain a standard error of 0.23 mm for the alignment process. It was assumed that the application of the rotational correction would make this estimate representative of the alignment process standard error averaged over the whole area of the film used for the NAT analysis.

4.5 DoseLab fluence comparison.

A fluence field comparison was performed using DoseLab to assess the difference in overlaid field images created by the treatment planning system (TPS) and the linear accelerator. For the assessment, fluence images from the TPS (computed) and from digitising film (measured) were overlaid and correlated. Digital films were aligned to match TPS images by rotating about marked locations, ePin for the TPS and pin pricking for film. Computed and measured images were overlaid using the MATLAB NORMXCORR2 function of DoseLab. Fluence evaluations were performed with DoseLab's NAT value using the combined uncertainties derived in sections 4.4.3 and 4.4.4. A result from a NAT was created to assess a simulated treatment field exposed on radiographic film. The NAT values show differences between computed and measured fields.

5 Results.

This chapter is comprised of results listed under subheadings that correspond to those of chapter 4 (Methods).

5.1 Digitiser characterisation.

5.1.1 Light source uniformity.

Figure 16 shows horizontal profiles from 20 digitisations of the template (UST). The left half of the figure shows the average of each horizontal profile location (3.6 cm, 12.5 cm and 21.4 cm) over the 20 digitised images. On the right is the coefficient of variation (CoV) for each location. Results are for the Exposure 12 setting. Results for Exposure 8 and 40 had essentially the same shape, and differed only in signal magnitude. The approximate average optical density value (OD × 20 000) for each setting is 21 000, 31 000 and 51 000 for 8, 12 and 40 Exposure. The figure illustrates a prominent centralised peak for the Exposure setting. The data also identifies the variation in optical density as the film passes through the device. This is shown on the graph from the magnitude variation between each measurement location (defined on the graph as different colours).

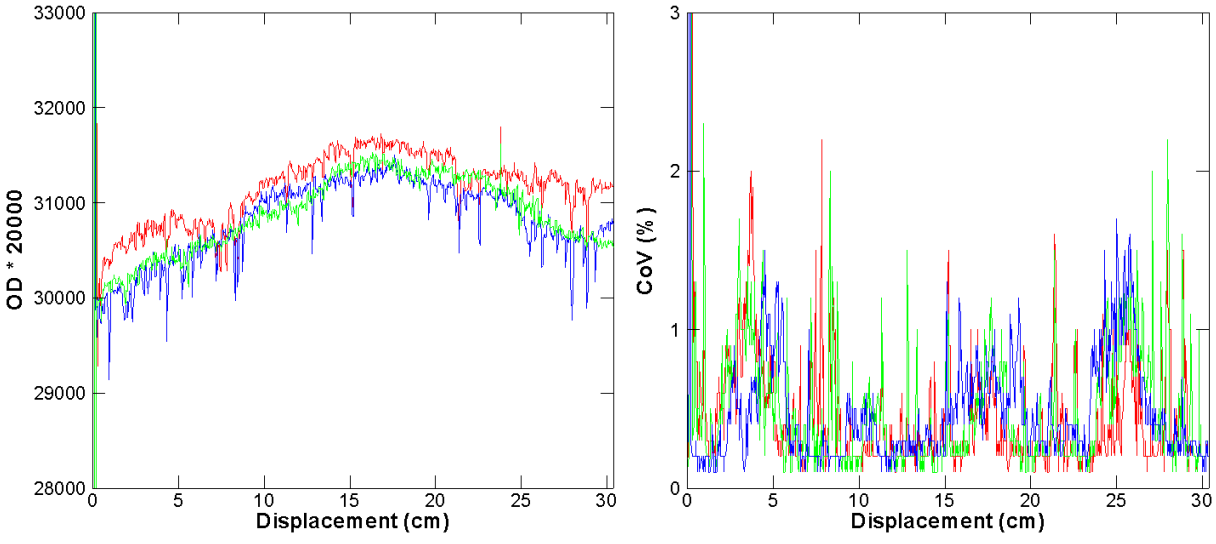

Horizontal mean Horizontal CoV

Figure 16. Plots for the optical density variation, with displacement i.e. uniformity, in the digitiser's light source (horizontal profiles). Averages are shown from digitising data collected at three measurement locations: red (top) 3.6 cm, green (middle) 12.5 cm, and blue 21.4 cm. Data is for Exposure 12 speed setting. The data also illustrates the variation of OD over the time it takes to scan the film since there exists an observable difference between profiles.

Figure 17 shows the mean optical density and the coefficient of variation for vertical profiles (locations 8.9 cm and 23.2 cm) from the 20 digitised images. These profiles show the variation in the digitiser's light output with time as the film passes through the device while being digitised. Results are for the Exposure 12 setting. Results for Exposure 8 and 40 had essentially the same shape, and differed only in optical density. The profiles differ in optical density because they were measured at two separate locations on the film that represent separate locations along the light source. This feature can be seen from the curvature of the graph in figure 16; if the OD is measured at 5 cm it will be less than if measured at 15 cm.

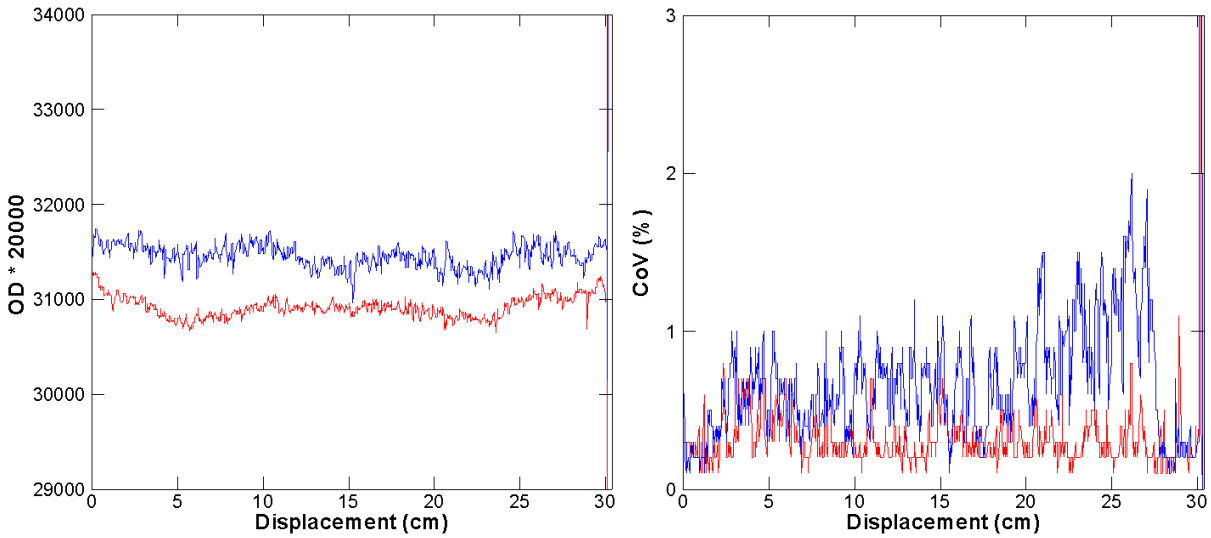

Vertical mean

Vertical CoV

Figure 17. Plots for the optical density variation, with time i.e. constancy, in the digitiser's light output (vertical profiles). Averages are shown from digitising data collected at two measurement locations: red (bottom) at 8.9 cm and blue at 23.2 cm. Data is for Exposure 12 speed setting. These profiles illustrate the variation in light optical density over time as the film is driven past the light source and receiver.

The two distinct profiles visible on the left hand side of figure 17 depict vertical profiles at different horizontal positions. They differ in magnitude because the intensity from the digitiser's light source varies along its length (figure 16). Figure 16 shows how profiles are influenced by the spatial variation of light intensity from the light source and somewhat of the variation in the density of the UST. There is a significant optical density variation with displacement as shown on the figure. There are slight differences observable at the three different measurement locations, but the general shape is the same; the peak appears at the same position and the intensity drops off on either side.

The central maximum is in the order of 5% higher than the OD at the edge of the film, whereas the average CoV is 1.3%. The variation with displacement is therefore statistically significant. Since the shape of the curve does not depend strongly on the vertical location of the line on the UST that it represents, variation in the optical density of the UST cannot be the most important cause. The shape of the graph must then represent spatial variation of the light source intensity. In 60 digitisations, it was found that the light intensity across the length of the light source was never uniform. This spatial variation of the light source has been observed by only one other investigator[w] who reported variations of 0.2 OD. However, the significant variation of light intensity is corrected by applying a uniformity correction file, a profile identical to the shape recorded in figure 16, to the output of the digitiser. Consequently, the distinctive curvature of the light source is removed.

Negative spikes are present in the red and blue profile in figure 16. The cause of these spikes is considered to be related to scratches on the film. Figure 18 illustrates the consequence of digitising a single film on a device that can be used to digitise multiple films. This results in film scratching because a feed roller, which is only operated during multiple film scans, remains stationary forcing the device to drag the film over an abrasive surface. Consequently, vertical scratches are created during digitising and can be seen most clearly in the red curve of figure 16 at approximately 6 cm and 11 cm displacement. The feed roller problem was subsequently circumvented by securing surgical cloth tape around the roller to allow the film to effortlessly slide past. Similar scratches occurred inside the digitiser on rollers because of the excess thickness of the UST, which was three times the regular film thickness.

Troughs can also be a result of data loss from grit located on the film during digitising. These troughs are localised to a small area (dust particle size) and appear at random locations. Other causes of extremes in the CoV appear at film edges, due to diffraction and scatter, and errors positioning the film in the digitiser.

[w] N. Childress, M. S. Ron Vantreese and I. Rosen, DoseLab 3.05 User Manual, http://doselab.sf.net/ (2003)

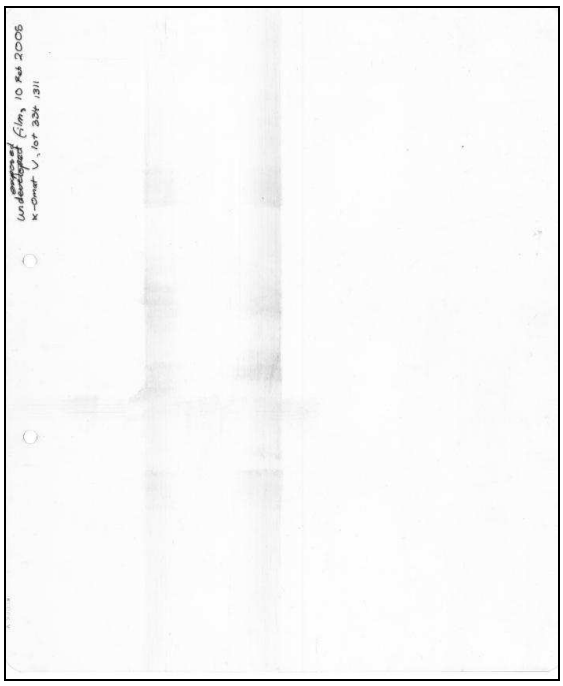

Figure 18. An image of when film gets damaged, feed roller damage, during digitising. The streaks in the central part of the image are created when the film catches on the multiple film feed roller which remains stationary during single film digitising.

Figure 17 shows profiles that are influenced by the temporal variation of the light output as the film passes through the digitiser and to a lesser extent the variation in the density of the UST. The variation of optical density across the film is of the order of 1.5%, much less than that observed in figure 16 (5%) and the average CoV is 0.4%. This shows that the temporal variation in the light source is not as significant as the spatial variation. The relative constancy of the vertical profiles is consistent with the conclusion made from the data in figure 17, that the variation seen in the horizontal profiles is caused by spatial variation of the digitiser light source intensity, not spatial density variations of the UST.

Films digitised without a correction for spatial uniformity of the digitiser light source will have areas located centrally appear relatively brighter. This means that dose comparisons using film analysis criteria could fail or pass unduly if not corrected.

5.1.2 Light source constancy.

Figure 19 shows the average OD through the large UST during a five-month evaluation. Average and CoV statistics were calculated from single profiles measured at 18.4 cm. The image was digitised using the Exposure 8 setting. Figure 19 also shows the coefficient of variation of the same horizontal

profiles. The average over all displacements for the coefficient of variation is 0.72%. A centralised peak is clearly visible in the images.

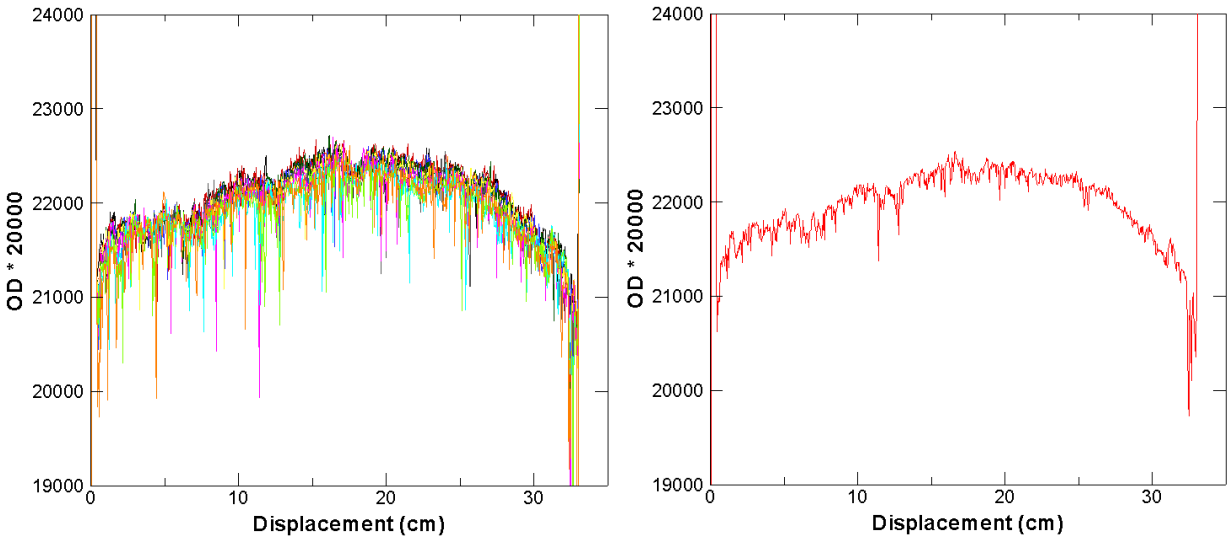

Horizontal constancy data

Horizontal mean

Figure 19. Plots for the variation in optical density, with displacement across the digitiser (horizontal profiles), during the five-month evaluation. Average data from 10 separate profiles is shown on the right; individual plots are shown on the left. Notice again the rise to a central peak in the centre.

During the five-month evaluation the general curvature of the horizontal profile remained relatively constant. As demonstrated in the right side of figure 19, the distribution of points is similar with respect to the variation of output over a short time as in section 5.1.1 (light source uniformity). The greatest deviation, on either edge of the profile, is from film edge uncertainty as is shown in figure 20. This suggests that a correction for uniformity need only be performed initially and can continue to be applied for at least five months. Mersseman and De Wagter (1998)[35] also evaluated a measurement error as a function of time and found, with respect to the coefficient of variation, that, "*comparing the short-term and long-term curves we concluded that the long-term reproducibility is also acceptable, especially below ODs of 2.0.*" Their short term and long term reproducibility were over one hour and four weeks. The CoV as measured by these authors was almost zero for OD less than one, 2% or less for OD up to 2.0, but greater than 5% for OD above 2.5. As with sections 5.1.1, literature regarding this uncertainty is difficult to find, but the average error measured here (CoV) of 0.72% agrees with the 1-2% error for the same OD as measured by Mersseman and De Wagter (1998).[35]

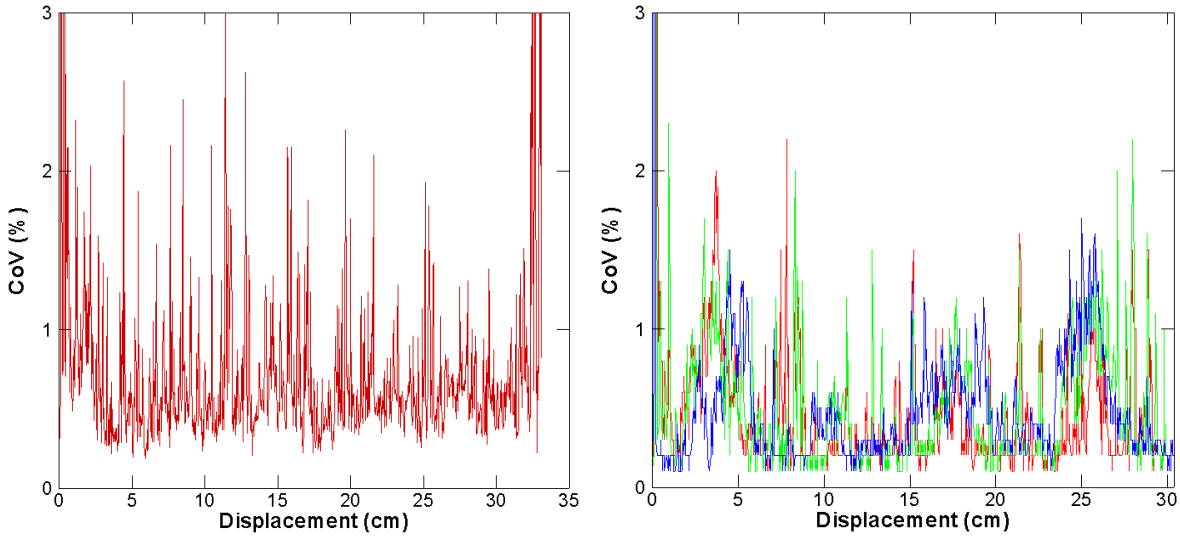

Distribution of constancy (CoV) Distribution of light uniformity (CoV)

Figure 20. Comparison of the distribution in OD between data collected for constancy and light uniformity. Pictured left, the distribution of points from 10 digitisations over a five-month period, and pictured right, the distribution of points from 20 digitisations taken on the same day (image reproduced from figure 17, section 5.1.1).

5.1.3 Geometric accuracy.

Tables 7 and 8 list the distance measurements between peaks of profiles made with Exposure 8, 12 and 40 of the displacement standardisation template (DST).

Table 7. Geometric accuracy measured in the horizontal direction.

Actual distance	Exposure 8		Exposure 12		Exposure 40	
	Profile 1	Profile 2	Profile 1	Profile 2	Profile 1	Profile 2
14.90	14.901	14.901	14.901	14.901	14.937	14.937
Difference (cm)	0.00	0.00	0.00	0.00	0.04	0.04

Table 8. Geometric accuracy measured in the vertical direction.

Actual distance	Exposure 8		Exposure 12		Exposure 40	
	Profile 1	Profile 2	Profile 1	Profile 2	Profile 1	Profile 2
14.96	14.866	14.866	14.901	14.901	14.866	14.866
Difference (cm)	-0.08	-0.08	-0.04	-0.04	-0.08	-0.08

In this study, a maximum error of 0.8 mm was measured over 15 cm in the vertical direction. There was no discernible trend of geometric accuracy with Exposure. Holmes and McCullough (1983),[55] using a line template and measuring the resulting converted X-Y plot, "*found it reasonable to expect*

± 1 mm or 1 % (whichever is greater) agreement on linear dimensions." The measured geometric accuracy of 0.8 mm is within the 3 mm tolerance for gamma analysis as recommended by Winkler et al. (2005)[6] and for radiographic film dosimetry as recommended by the AAPM.[1]

5.2 Film processor characterisation.

Figure 21 shows the results for OD-to-dose curves obtained for the radiographic film and for the radiochromic film measurements. The error bars were calculated as half the resolution of the digital readout on the densitometer but excluded from the plots because they could not be seen.

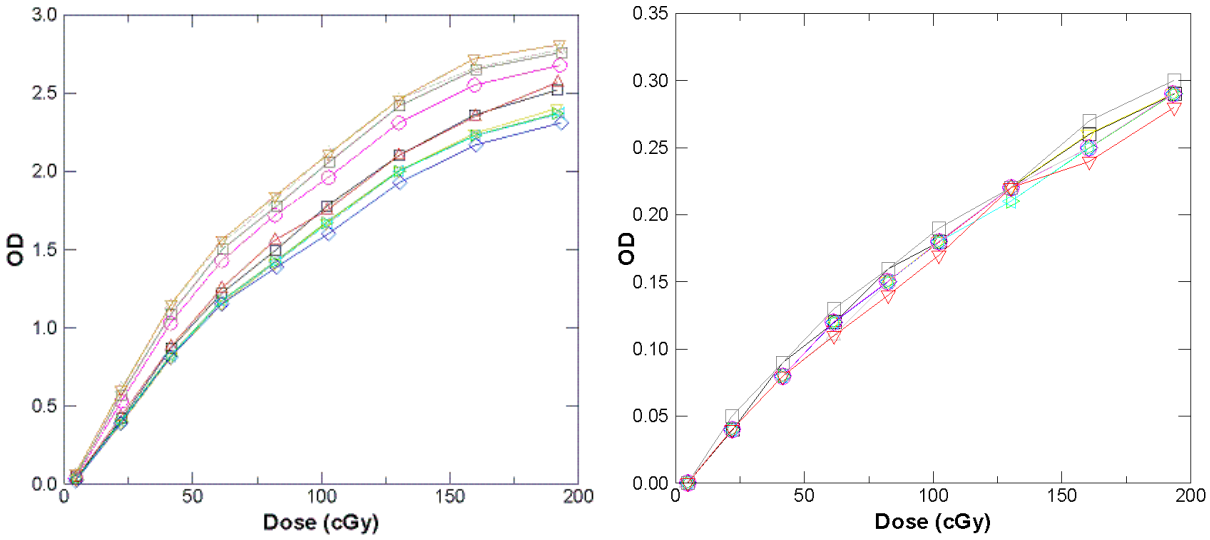

Radiographic OD-to-dose

Radiochromic OD-to-dose

Figure 21. OD-to-dose curves, created from measurements made on 10 separate days. The plots on the left were measured on radiographic film and on the right for radiochromic film. Notice the divergence of points with higher doses for the radiographic sets as a result from processing error. Notice also the reduced OD for the radiographic film as a result from a decreased sensitivity to radiation. Error bars would represent half of the minimum resolution for each digitiser (0.005 OD). The error bars are smaller than the symbol shapes and therefore were omitted from the graphs.

Table 9 lists the minimum and maximum OD and the coefficient of variation for radiographic film (processing included) and for radiochromic film (no processor involved) at each measurement location as described in section 4.2. The second row of the table shows the magnitude of dose delivered at the centre of the field corresponding to each location. The actual dose delivered at each location is higher because scatter from the other fields is included, as noted in section 4.2. Ion chamber results are also listed for comparison.

Table 9. Comparison between radiographic and radiochromic film OD variation.

Measurement location	O	A	B	C	D	E	F	G	H
Output (cGy)	0	20	40	60	80	100	130	160	190
Min dose (cGy)	4.41	21.94	41.41	61.08	81.72	101.83	129.90	159.41	191.34
Max dose (cGy)	4.81	22.50	41.71	61.52	82.59	103.20	130.79	160.41	193.56
Dose CoV	3.5%	0.3%	0.1%	0.2%	0.2%	0.2%	0.1%	0.1%	0.1%
Min OD (radiographic)	0.02	0.41	0.81	1.15	1.42	1.65	1.94	2.17	2.35
Max OD (radiographic)	0.07	0.67	1.20	1.59	1.89	2.18	2.46	2.71	2.86
OD CoV (radiographic)	39.4%	19.3%	15.3%	13.0%	11.5%	11.1%	9.5%	8.4%	7.3%
Min OD (radiochromic)	0.00	0.03	0.07	0.11	0.14	0.17	0.20	0.25	0.28
Max OD (radiochromic)	0.01	0.05	0.09	0.13	0.16	0.19	0.23	0.26	0.30
OD CoV (radiochromic)	105.4%	15.9%	8.3%	6.5%	4.5%	3.7%	4.5%	2.0%	2.3%

Figure 21 shows a significant difference in OD for radiographic films processed on different days. Between set 1 (2nd June) and set 10 (28th Sep), 11% OD variations were observed for 80 and 100 cGy and up to 19% for 20 cGy. An uncertainty of 11% exceeds an acceptable 5%[6] tolerance limit that would be required for a patient plan evaluation. However this is not uncommon, Bucciolini et al. (2003)[8] also noticed large variations in optical density between processing days and from six samples they recorded an error of 15%.

The CoV for the ion chamber dose measurements is shown in table 9 (labelled as "Dose CoV"). This is less than 0.3% over the course of the experiment for all points except for location O. At location O, the measured dose is very low, resulting in a high CoV, although the difference between the maximum and minimum readings is only 0.4 cGy. This confirms that variation in linear accelerator output is not the cause of the differences in OD on different days.

The CoV for the radiochromic film OD is on average less than that for the radiographic film, with a minimum CoV of 2.0% compared to 7.3% for radiographic. Since the radiochromic film is self-developing, it is concluded that film processing is the major contributor to the total radiographic film dosimetry uncertainty. Robar and Clark (1999)[19] measured 1.1% errors between processing films on the same day with identical exposures. For films processed on separate days, they found variations of 2.9%. Uncertainties in film processing are unavoidable though some processors perform better than others. Novotny et al. (1997) [53] found a processing reproducibility of 0.65% with their newer

processor (AGFA Curix 260) though for their older processor (AGFA Gevamatic 1100) the variation was between 1.6% and 3.8%. Robar and Clark used a film processor that had a high throughput and regular quality assurance performed daily. They monitored processing conditions and suggested that, "*developer temperature fluctuated by less than ±0.5 °F between processing sessions.*"

The temperature of the film processor used in this study was not directly monitored and the throughput was very low. As discussed in section 2.6, film processing temperature is a key ingredient in the development of an image. Unfortunately, the film processor was part of another department and thus maintenance by the Physics staff was not allowed. Consequently, the lack of quality assurance and infrequent use of the film processor is the main cause for the large variation in OD seen in figure 21 when processing films.

The AAPM TG 69 report[1] recommends monitoring developer temperature by using an external source. Since the temperature of the developer plays an important role in OD variations, processors maintain a temperature variation to within 0.3 °C. [1] The report also mentions monitoring the time it takes to process the film (immersion time) and monitoring the concentration of the processing chemicals. These recommendations are highly valid. However, the document does not offer a solution if such criteria are not reached. Several options are available on automated processors: (1) replace the processor, or (2) perform maintenance on the processor. Replacing a costly item was not considered practical and maintenance of the processor was performed by a qualified Kodak engineer as per a contractual agreement. The expertise of a trained product engineer was not under consideration. Hence, the processor functionality was considered to be within manufacturer specifications (± 0.3%). In any event, monitoring the temperature, immersion or chemical concentration variations do not solve the problem of OD variation it only identifies them.

In addition, the Victoreen densitometers are limited to two decimal places which inhibit the resolution at low optical densities. This is more significant for the radiochromic film, because of its lower sensitivity, which is significant for lower doses in the film. However, at higher doses, the coefficient of variation is much lower for radiochromic than radiographic film, which is due to the magnification effect in radiographic film processing and subsequent magnified uncertainty.

A daily sensitometry check[1] was also considered as part of the QA process although this, just like temperature and immersion time monitoring, would only identify a problem and not offer a solution. To solve the problem, an OD-to-dose curve was considered as part of regular QA.

Consequently, this increases the time needed for each patient and was therefore considered impractical for high patient loads.

5.3 Radiographic film characterisation.

5.3.1 Base plus Fog.

Figure 22 shows Base plus Fog removal of a standard 10 cm × 10 cm field. The central high dose region, pictured on the right of the peak, demonstrates the correction for the non uniformity of the light source. The peripheral low dose region demonstrates the Base correction.

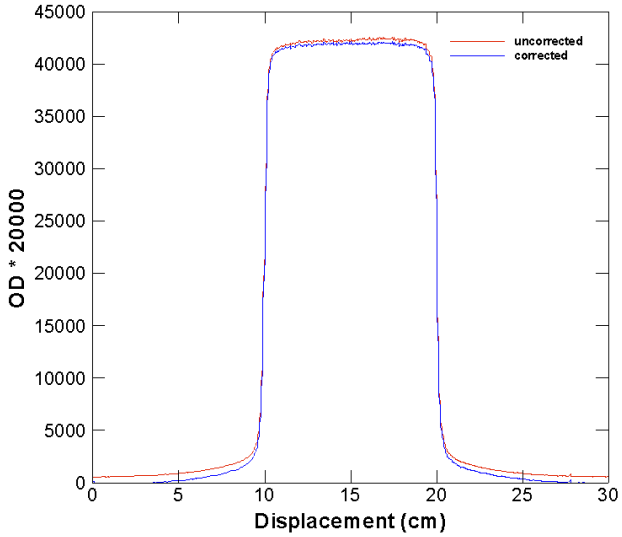

Figure 22. Corrected and uncorrected horizontal profiles through a film exposed to a 10 cm × 10 cm field of 6 MV photons at 1.5 cm depth. Notice how the uncorrected profile (top profile) deviates from the corrected from left to right. This occurs because the intensity of the light in the digitiser is different at the centre compared to that at the periphery.

Even with the first step of the method for correcting Base plus Fog described in section 4.3.1 (using the Exposure setting of the digitiser) and as shown in figure 22, the uncorrected profile does not reach zero outside the field. The OD is 1.3% at 10 cm outside the field. When the uniformity correction in DoseLab is applied the corrected profile tapers away slowly reaching 0.5% at approximately five cm outside the field.

Radiation dose outside the field arises from leakage and scattered photons from the linac, from the air in-between film and linac, and from scatter within the phantom. Leakage radiation from the linac

is very small, typically below 0.1%.[x] The contribution of scattered photons from within the phantom depends on the thickness of build-up and the distance from the field edge. For the setup used to expose the film shown in figure 14, ion chamber measurements suggest that the total dose at 10 cm outside the field is 0.5%. This cannot account for the 1.3% OD seen 10 cm outside the field on the uncorrected profile in figure 22. Consequently, this OD primarily results from Base plus Fog. The reduction to 0.5% at 5 cm outside the field demonstrates that using the two steps methodology as described in section 4.3.1 does indeed correct for Base plus Fog.

5.3.2 Dose rate dependence.

Table 10 lists the results from ImageJ's region of interest statistics for the film dose rate dependence analysis.

Table 10. Radiographic film dose rate dependence with rates of 200 cGy/min and 600 cGy/min.

Set	Fraction	Mean reading (raw)		Comparison to 600 cGy/min
		200 cGy/min	600 cGy/min	
1	1 × 60 cGy	43280	43016	100.61%
	2 × 30 cGy	43516	43159	100.83%
	3 × 20 cGy	43717	43386	100.76%
2	1 × 60 cGy	45731	46714	97.89%
	2 × 30 cGy	45715	46460	98.40%
	3 × 20 cGy	45769	46217	99.03%
3	1 × 60 cGy	46269	46738	98.97%
	2 × 30 cGy	46309	46351	99.91%
	3 × 20 cGy	46790	45806	102.15%

Table 11 lists the dose rate dependence for the ion chamber.

Table 11. Ion chamber dose rate dependence.

Set	Fraction	Mean reading (nC)		Comparison to 600 cGy/min
		200 cGy/min	600 cGy/min	
1	1 × 60 cGy	13.119	13.049	100.54%
	2 × 30 cGy	13.117	13.068	100.38%
	3 × 20 cGy	13.117	13.073	100.33%

[x] Varian Medical Systems, *Clinic 1800, 2100C(/D), 2300C/D, 21EX, 23EX, iX, & Trilogy Radiation Leakage Data*, (Radiation Safety Office (RSO 22), Palo Alto, 2006)

The intensity of films exposed at 200 cGy/min agreed within 2.1% with those exposed at 600 cGy/min, as shown in table 9. There appears to be no discernible trend, since the 600 cGy/min films give a higher reading on some days and lower on others. The ion chamber results for set 1 (table 11) show a consistently higher reading for 200 cGy/min, with a maximum difference of 0.5%. On the same day, the film results range between 1% lower to 2% higher (set 3, table 9). Martens et al. (2002)[13] recorded a very small dose rate dependence finding that there was a relationship between dose rate and optical density. However, this dependence was minimal, about 0.03 OD between 600 cGy/min and 100 cGy/min. This suggests that the variations in film intensity are due to processing differences rather than dose rate dependence. This is confirmed by the discussion in section 5.2 where it was concluded that the film processor introduces a significant uncertainty.

Dose rate dependence in this experiment was tested by varying the linac repetition rate. During IMRT treatment, the dose rate may be controlled by varying both the linac repetition rate and the dose per pulse. However, the time constant for unstable latent pre-image centre formation and decay is known to be larger than the linac micro-pulse length,[80] so varying the repetition rate is a valid method for testing film dose rate dependence.[81]

5.3.3 Dose fraction dependence.

The results for the radiographic film fraction dependence for two dose rates (200 cGy/min and 600 cGy/min) are shown in tables 12 and 13. The values listed are results obtained from ImageJ's region of interest evaluation.

Table 12. Radiographic film fraction dependence for 200 CGY/min.

Set	Statistic	1 × 60 cGy	2 × 30 cGy	3 × 20 cGy
1	Mean reading (raw)	43280	43516	43717
	Diff. from 60 cGy	-	100.55%	101.01%
2	Mean reading (raw)	45731	45715	45769
	Diff. from 60 cGy	-	99.97%	100.08%
3	Mean reading (raw)	46269	46309	46790
	Diff. from 60 cGy	-	100.09%	101.13%

Table 13. Radiographic film fraction dependence for 600 cGy/min.

Set	Statistic	1 × 60 cGy	2 × 30 cGy	3 × 20 cGy
1	Mean reading (raw)	43016	43159	43386
	Diff from 60 cGy	-	100.33%	100.86%
2	Mean reading (raw)	46714	46460	46217
	Diff. from 60 cGy	-	99.46%	98.94%
3	Mean reading (raw)	46738	46351	45806
	Diff. from 60 cGy	-	99.15%	97.98%

Tables 14 and 15 list the ion chamber fraction dependence results.

Table 14. Ion chamber fraction dependence for 200 cGy/min.

Set	Statistic	1 × 60 cGy	2 × 30 cGy	3 × 20 cGy
1	Mean reading (nC)	13.119	13.117	13.117
	Diff. from 60 cGy	-	99.98%	99.98%

Table 15. Ion chamber fraction dependence for 600 cGy/min.

Set	Statistic	1 × 60 cGy	2 × 30 cGy	3 × 20 cGy
1	Mean reading (nC)	13.049	13.068	13.073
	Diff. from 60 cGy	-	100.15%	100.19%

The variation between films exposed with two fractions compared to one varies by approximately 1%. For three fractions to one, the variation is the same except for one measurement that varied by 2%. For the ion chamber measurements these values are 0.02% for 200 cGy/min and 0.2% for 600 cGy/min. Martens et al. (2002)[13] showed that optical density is reduced by as much as 3.2% for ten fractions and that the reduction is proportional to the number of fractions. They suggest this phenomenon is related to an interaction lag between the radiation and the film grains during the initial stages of irradiation and thus is compounded with multiple exposures. However, they found no significant fraction dependence effect when considering the range of time intervals between segments of their IMRT fields with their Elekta[y] accelerator. Therefore, as in section 5.3.2, it is concluded that film processing variations outweigh any variations due to dose fraction dependence.

[y] Elekta, Stockholm, Sweden.

5.3.4 *Film homogeneity.*

Figure 23 shows uncorrected horizontal profiles for two film batches. Profiles illustrate Base plus Fog and light source uniformity values for Exposure 12. The average difference between profiles is 0.18%.

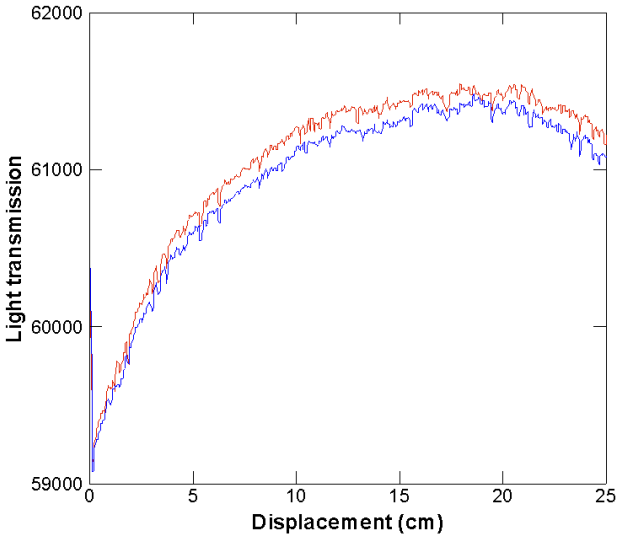

Figure 23. Base plus Fog profiles from two film batches; batch 334 1311 (bottom red) and 335 1181 (top blue) are shown. Curvature of the profiles is a result from the uniformity in the digitiser's light output. Data shown is from the raw output of the digitiser using the linear translation table.

The difference in intensity between the two film batches seen in figure 23 is less than the variation of intensity at different location on the same films as shown in figure 16. This suggests that there is no significant film heterogeneity between the batches tested. In figure 23, average variation in OD between the two film batches is small (0.18%). This uncertainty is relatively smaller than Robar and Clark (1999)[19] measurement of 0.85% OD variations between same batch films, but insignificant when compared to the total uncertainty (section 5.4.1).

5.4 *Error analysis.*

5.4.1 *Film dosimetry uncertainty.*

Table 16 lists the uncertainties from each of the characterisation sections, using the methods outlined in chapter 4.

Table 16. Radiographic film dosimetry uncertainties.

Uncertainty	Section	Magnitude
Light source uniformity	5.1.1	0
Light source constancy	5.1.2	0.72%
Geometric accuracy	5.1.3	0
Film processing	5.2	11.0%
Base plus Fog	5.3.1	0
Dose rate dependence	5.3.2	0
Fraction dependence	5.3.3	0
Film homogeneity	5.3.4	0.18%
Linac output (symmetry)	5.4.2	2.00%
Total uncertainty	**5.4.3**	**11.2%**

5.4.2 Linac dosimetric uncertainty.

The dosimetric uncertainty for the linear accelerator was taken from the centre's field symmetry tolerances, which conforms to ±2.0%.

5.4.3 Overall dosimetric uncertainty.

Equation 7 shows the calculation for the overall dosimetric uncertainty.

$$total = \left[(film)^2 + (processor)^2 + (digitiser)^2 + (linac)^2\right]^{\frac{1}{2}} \quad [7]$$

$$total = \left[(0.72)^2 + (0.18)^2 + (11.0)^2 + (2.0)^2\right]^{\frac{1}{2}} = 11.2\%$$

5.4.4 Geometric uncertainty.

Geometric uncertainties were added in quadrature. This incorporated 0.8 mm from geometric accuracy (section 5.1.3), 0.5 mm from Varian MLC positioning error[79] and 0.23 mm for film alignment error (section 4.4.4). The results are listed in table 17.

Table 17. Radiographic film geometric uncertainties.

Uncertainty	Section	Magnitude
Geometric accuracy	5.1.3	0.8 mm
MLC positioning	5.4.4	0.5 mm
Film alignment	4.4.4	0.23 mm
Total uncertainty	**5.4.3**	**0.97 mm**

5.5 Practical implications in the OD-to-dose calibration uncertainty.

To ascertain the uncertainty associated from film processing**,** a comparison was made between a field exposed on radiographic film then converted to dose using two different OD-to-dose calibrations. The difference between the two resulting dose images would then be used to make an assessment of the uncertainty contributed by film processing to the overall uncertainty. The two OD-to-dose calibrations were chosen from two of the ten calibrations described in section 5.2 and were those which had the greatest OD differences for similar doses.

The two separate OD-to-dose calibrations were used to convert the OD file of the digitised film into two separate dose images. Figure 24 shows dose differences in mGy between the two dose images using DoseLab and figure 25 shows the distribution of the dose differences.

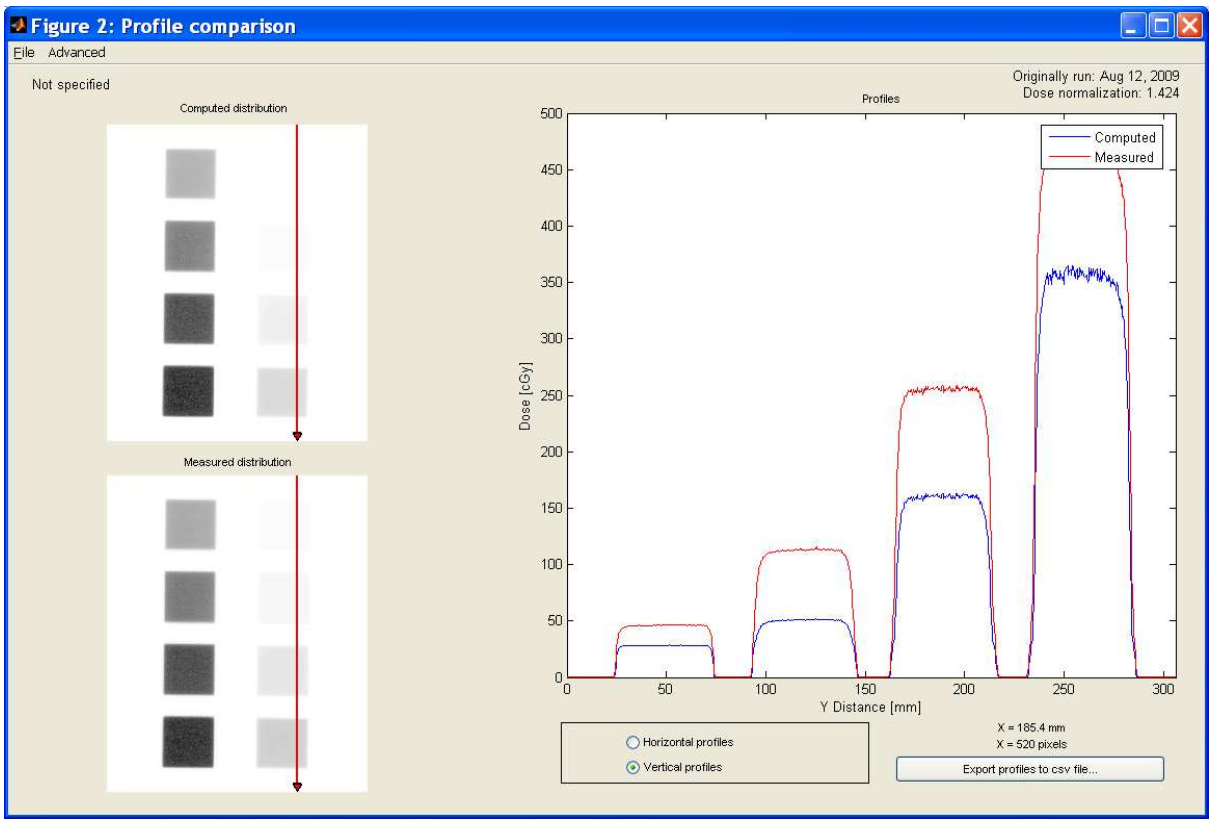

Figure 24. DoseLab's "Interactive Profiles" option showing dose differences (in mGy) between images created using different OD-to-dose calibrations. The DoseLab software incorrectly labels the y axis units as cGy, and this is faithfully represented in the image, but it has been verified that the correct units are mGy. Both images on the left were created from the same film; they were spatially correlated so there was no need to use the MatLab function for a best fit approximation. Accordingly, the "Tif to Tif – already registered" option was selected in DoseLab. One image was normalised to the other at the 190 cGy location (location H). A dose maximum of 192.53, which was the maximum measured dose in the OD-to-dose calibrations, was used for statistical normalisation. Statistics were determined from the histograms DoseLab created.

The left side of figure 25 shows the percent error variation, expressed as a percentage of the particular value, for discrete dose values. Each discrete optical density is mapped to two separate doses from two separate OD-to-dose conversions. The percentage difference from the first dose conversion is compared to the second dose conversion. The discrete point densities are the same as those used for the OD-to-dose curves plotted on the left side of figure 21.

The right side of figure 25 shows the frequency of percent differences with respect to a maximum dose (192.53 cGy) for a comparison of a dose map created with two different OD-to-dose conversions. The spike at zero percent represents the greatest number of pixels. No point on the discrete dose difference plot has a relative percentage error less than 20%. Therefore, these points

must arise overwhelmingly from outside the irradiated area and receive a low dose. Hence, the dose difference as a percentage of the maximum is quite low. The low frequency of points with percentage differences close to zero percent confirms that there are only a very small minority of points with values in these regions.

The second most frequent percentage difference is in the homogeneous high dose region with a dose just below maximum, which has a percentage difference of 20% of the dose maximum or higher. The other percentage differences all have very low frequency, and so can be disregarded. These points would in any case tend to be from high dose gradient penumbral regions (hence the low frequency) and likely to be passed by the 3 mm distance to agreement criteria in the NAT analysis anyway.

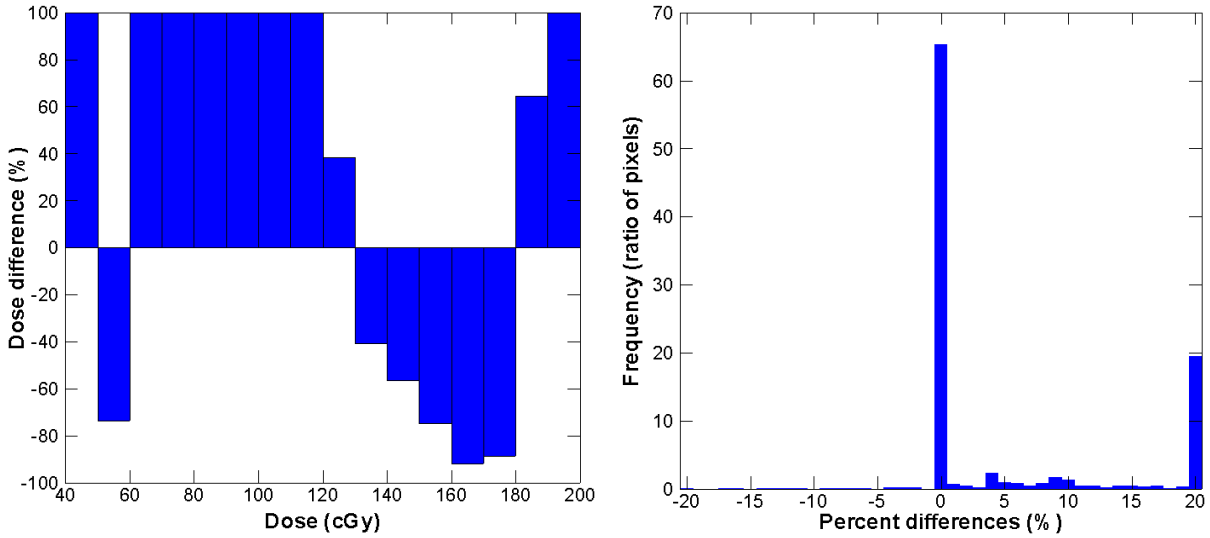

Dose differences of the local dose

Dose differences of the maximum dose

Figure 25. Absolute and relative dose differences, relative to 192.53 cGy, for a field converted using two different OD-to-dose calibrations.

For NAT analysis, it is the absolute percent error in the high dose region that is of significance. The average absolute percentage difference is of the order of 20%. Since this was the worst case estimate obtained from a sample of 10 points, it is appropriate to apply some statistical analysis to determine the standard error for the processing of a single film. If we assume that the result of a film processing is normally distributed about a mean half way between the two extremes, then after sampling the distribution 10 times we have observed that all points are between 0.9 times the mean

and 1.1 times the mean. If the standard error is 5.5%, the probability of observing all 10 points within the range is 0.5, so this value is taken as estimate of the standard error.

Confirming a Gaussian distribution would have identified that this uncertainty was random, but would have required a large number of repeated calibrations. Of principle interest to the author was the magnitude and dosimetric consequences of the largest discrepancy observed within the dataset acquired. Therefore, an upper bound on this error was estimated by studying the two measurements that differed by the greatest amount

The uncertainty for the dose rate and fraction dependence was considered to be insignificant. The variation seen in these analyses was attributed to film processing and so is excluded from the overall film dosimetry error to avoid duplication.

5.6 DoseLab fluence comparison.

Figure 26 shows NAT values for a simulated IMRT field with 10% and 3 mm acceptance criteria. For this comparison, 59.7% of points pass the DD criterion and 95.4% pass the DTA.

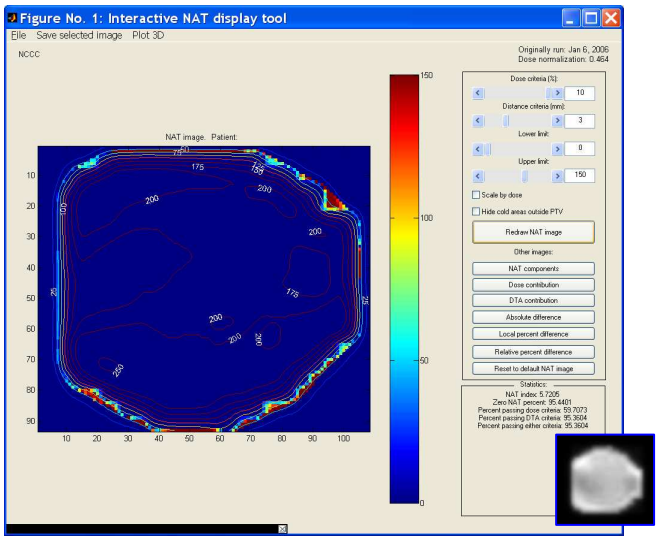

Figure 26. An IMRT fluence comparison in DoseLab. Points failing both acceptance criteria are illustrated in yellow, orange and red. Colours depict failing severity with red (peripheral field) the largest error. Insert illustrates the original Computed fluence. Note the image is mostly blue and nearly all points pass.

The combined uncertainty of 10% was used in the fluence comparison, even though the 11% two sigma value of the uncertainty associated primarily from film processing was higher, because 10% was the largest percent difference DoseLab would allow. A 3 mm distance-to-agreement was also used instead of the measured uncertainty of 0.97 mm because this value was considered an acceptable tolerance criterion.[1]

The problem of excessive uncertainty associated primarily from film processing could theoretically have been overcome by taking a calibration curve immediately prior to the test, and immediately after. This option was dismissed as impractical in clinical practice. The extra time taken for this process in a radiotherapy department would make it impossible to achieve the required benchmark of two weeks from initial consultation to commencement of treatment. There is no surety that the processor would have produced acceptable results, which would require a CoV derived from the two calibrations of 2.11%.

While 3 mm is a standard value used in clinical practice,[6] a dose difference as large as 10% is greater than any found in any published clinical practice. The NAT analysis has been performed and documented purely to facilitate the discussion of the clinical significance of the extraordinarily large dose difference, which forms the central focus of the concluding chapter.

5.7 Further discussions.

For this study the greatest uncertainty originates from film processing (11%). To understand why such a large uncertainty was measured is to understand the image formation method. The nature of radiographic film processing could be perceived as a magnification process.[40] Small variations introduced in the initial stage can result in large uncertainties at the end. To ensure the correct gain is repeatable the film processor must maintain constant temperature, speed of processing and active chemical concentration. Some film processors can achieve a limited intra session variability: Danciu et al. (2001)[15] measured an uncertainty of 1% while Novotny et al. (1997)[53] measured 0.65% for their newer processor and 1.6% to 3.8% for their older one. However, as shown in this study and by Bucciolini et al. (2004),[8] variations greater than 10% are possible for film processed on separate days. In addition, the processors considered in this study where old, one with a low throughput of films and the other with a high throughput, and this age can influence its ability to control the key areas of image formation.

To reduce the uncertainty for the processor used in this study, the temperature, speed of processing and the active chemical concentrations would need to be manually controlled. This is probably more impractical than more difficult since the purpose of most film processors is to portray contrast not measure dose. The application of such an ideal processor creates more work for the user than necessity requires; the main reason why automatic processors are used is because of their convenience. While the magnitude of the processing uncertainty has been measured, and some strategies for reducing it have been identified, e.g. feeding a few extra films through at a time, using another film like radiochromic film or AGFA Structurix D2, or replacing the processor altogether. A detailed investigation has not been performed as part of this study, but might form the basis of a future study of its own.

6 Conclusion.

"*To improve is to change; to be perfect is to change often.*" – Winston Churchill

The aim of this work was to evaluate the use of radiographic film, an already existing relative dosimeter, as an absolute dosimeter for intensity modulated radiotherapy (IMRT) at the Nepean Cancer Care centre. Previous studies have shown that this must be done on an individual basis for particular combinations of facilities, equipment and procedures. This thesis presents the first such evaluation of the possibility of conducting radiographic film IMRT dosimetry at the centre.

Radiographic film cannot be used as an absolute dosimeter at the Nepean Cancer Care centre for plan evaluations if the equipment described in this study is used. An uncertainty of 11% for film processing exceeds an acceptable tolerance criterion of 5%,[6] which would be needed for an acceptable plan evaluation. Using such a processing uncertainty would exceed dose recommendations set by the ICRU[62] for a prescribed dose. Indeed, using a dose difference of 10% renders the whole NAT analysis pointless from a clinical point of view, but it has been performed and documented here for completeness.

During fluence comparisons it is essential that film processing is redefined for each measurement day, an alternative film processor is used, or a different type of film such as radiochromic or perhaps AGFA Structurix D2 is used. Informative fluence comparisons are possible with the existing processor, although significantly reduced in utility because of marginal uncertainties. These comparisons can prove only generalised field shape equivalence, and do not contain the dosimetric information that IMRT QA requires. To improve fluence comparison conditions the following essential criteria must be met:

1. A new film processor capable of reducing uncertainty to no greater than one percent or a simple method of redefining the optical density and dose relationship for each individual QA examination,
2. An auto-developing film such as radiochromic with the capability for measuring dose linearly between 0 and 300 cGy,
3. An intuitive program able to perform routine film analysis and fluence comparisons quickly, easily and with certainty.

If option 1 is satisfied then the uncertainty could be significantly reduced from 11% to 2%.[53] Consideration towards the purchase of a new film processor would be recommended over the extra work required in redefining the optical density and dose relationship for each QA patient. However, consideration to other types of films, particularly radiochromic, could offer more satisfaction and also reduce the need for a film processor.

With these things in place, film dosimetry could be implemented to enable an IMRT program at the centre and would be highly valued in the department. The initial cost of establishing film dosimetry solely to support IMRT would be prohibitive for some departments, and would delay implementation of IMRT until necessary acquisitions could be accommodated within the departmental budget. Fortunately most radiotherapy departments already have active relative film QA programs and thus could possess the necessary equipment needed for IMRT QA analysis, and costs can be reduced when such circumstances arise. At the Nepean Cancer Care centre, the existing processor cannot be utilised in an IMRT QA program, and efforts to do so have conceivably delayed the introduction of an IMRT program more than any budgetary constraints ever would have.

Radiographic film may not yet share the same importance as ionisation chambers and solid state detectors although through necessity its role in IMRT QA may one day surpass these measuring instruments. Measurements that introduce large uncertainties would have to be minimised and new technologies introduced or old technologies improved or adapted to fulfil such a need. As the acceptance criteria are mandated by clinical requirements, one very important consideration is that as measurement error increases, so does the probability that deliverable treatments will erroneously fail acceptance criteria. This will interfere with the efficacy of patient treatment by potentially increasing the time between initial consultation and the commencement of a course of IMRT. Of greater concern is the less frequent possibility that a proposed IMRT treatment that is not delivered as prescribed by the IMRT delivery modality will nevertheless pass the IMRT QA acceptance criteria because the discrepancy has been erroneously reduced by measurement error.

To put this endeavour in context, radiotherapy is a vibrant discipline; it is always challenging with new devices and techniques being developed continuously. A great deal of passion and thoughtfulness goes into every treatment from a multi-disciplinary team. To even begin to plan this project required many involved discussions with colleagues at the Nepean Cancer Care centre, at a time when the introduction of IMRT in Australia was still not widespread. The combination of

radiotherapy modalities and techniques makes quality assurance a never-ending challenge. Hence, every treatment procedure is unique. Monitoring and developing quality assurance practices that cover and control for all possibilities is highly demanding. Although with every new challenge brings an equally innovative solution. In the time that has passed since this work was begun, the practice of IMRT within Australia has matured, but film dosimetry is still a competing technology for the implementation of IMRT and the complexities that it comprises; it may yet emerge as the preferred option.

7 Glossary.

AAPM	American Association of Physicists in Medicine.
Absorbed dose	A measure of ionising radiation magnitude (Gy) that can be calculated from exposure. Absorbed dose is used to describe all types of ionising radiation, the quality of that radiation, and for all materials.
ARPANSA	Australian Radiation Protection and Nuclear Safety Agency. Their functions include maintaining the primary standard for radiation dosimetry in Australia, and calibration of radiation dosimeters.
Backscatter	A region within a phantom beyond a measurement point. The reason for backscatter is that it provides a more accurate measure of dose at the measurement point.
Beam	See *field.*
Build-up	A layer of phantom that is used to allow a measurement point to reach a specific dose. In some situations, the desired dose is a maximum value. For all other situations, the requirement is to reach a dose reference. Build-up exits within a phantom between the phantom's surface and the measurement point. The "build-up region" is an area defined anywhere between the phantom surface and a depth of dose maximum.
Collimator	A collimator is a system of radiation shields. Primary collimators are purely used to trim stray radiation. Secondary and tertiary shields are used to vary the size and shape of a field. Jaws are considered secondary collimators and MLC tertiary.
DD	Dose Difference (%). One of two main analysis criterion of 2D dosimetry when comparing overlaid fluence images. It is a measure of the percent difference of one pixel's magnitude on one image compared to a pixel directly beneath it in another image.
Densitometer	A simplified version of a digitiser, which is limited to measuring one or a few points at a time. The Victoreen models 07-424 and 07-443 densitometers were used in this project. They are both single point measurement devices.
Digitiser	A device that measures light attenuation through a transparency. The Vidar VXR-16 DosimetryPRO is a digitiser somewhat similar to a flatbed scanner

	only it is more accurate, more precise and has better resolution. The digitiser contains a broadband UV light transmitter and a charged coupled device (CCD) receiver. The CCD is a matrix of photodiodes where the photodiode is a semiconductor. The matrix of photodiodes and the UV light form the transmitting and receiving device.
dpi	Dots per inch.
DST	Displacement Standardisation Template, a term created for use in this project. A clear template created from a single unexposed Kodak radiographic film. Markings from a felt-tipped pen were drawn on the template using a line plotter to create measureable distances that were digitised.
DTA	Distance-to-Agreement (mm). One of two main analysis criterion of 2D dosimetry when comparing overlaid fluence images. It is a measure of the distance from one pixel on one image to a nearby pixel with similar magnitude on another image.
Exposure (digitiser)	A setting of the Vidar VXR-16 DosimetryPRO digitiser. This setting changes the speed that the film travels through the device. The slower the speed (higher Exposure setting number), the lighter the digitised image.
Exposure (film)	A magnitude of radiation delivered to a film.
Exposure (measure)	Exposure is the measure of charge produced in air by electrons per unit mass, $X = dQ/dm$, and is measured in Coulombs.
Field	A radiation volume, magnitude and direction. Many linac parameters make up a field including collimation, energy and time.
Fluence	Photon fluence is the number of photons that enter a cross-sectional area. Fluence is the radiation flux integrated over time.
Gray (Gy)	A unit of measure for absorbed dose, given in Joules per unit mass (J/kg).
Gy	See *Gray*.
IMRT	See *intensity modulated radiation therapy*.
Intensity Modulated Radiation Therapy (IMRT)	A distinctive type of treatment in radiotherapy that utilises an MLC in a way that creates fields within fields. This is more conformal than regular treatment. IMRT is also sub divided into "Step and Shoot" and "Sliding Window" techniques. In the latter, the MLC moves continuously while the radiation is delivered. The former moves the MLC into discreet positions while

	the radiation is paused to allow the MLC to move to the next position.
Jaws	A set of four tungsten blocks approximately eight cm thick used to create a field.
Linac	See *linear accelerator.*
Linear accelerator (linac)	A device capable of creating ionising radiation in two distinct forms, electron and photon beams (fields). The type of linac used in here was manufactured by Varian (models 21EX and 2100CD).
MLC	See *multileaf collimator.*
Monitor Unit (MU)	A measure of output from a linear accelerator.
MU	See *monitor unit*.
Multileaf collimator (MLC)	A dynamic shielding system comprised of many shields (leaves) that move independently of each other to create different shapes. The Varian Millenium MLC has 120 leaves, 60 on each side (bank) of which 20 are approximately 0.5 cm thick and 40 are approximately 1 cm thick.
OD	See *optical density*.
OD-to-dose curve	A plot of absorbed dose versus OD. These curves show the sensitivity of the measuring device (film) with dose.
Optical density (OD)	Optical density is a measure of optical attenuation, it is the log of the difference in optical signal from the source (I) to the receiver (I_0), $OD = \log(I/I_0)$.
Penumbra	The penumbra is a region at the edge of a field where the dose gradient is steep. It occurs at the edge of the collimator. The dose gradient is a result from partial transmission through the collimator and diverging ray line paths from a finite sized radiation source.
Phantom	In radiotherapy, a phantom imitates the characteristics of water i.e. it has similar scattering and absorption properties of water. It replaces water for convenience because it is solid at room temperature and can be handled with ease. Water is used because of its similarities with human tissue.
Processor	An automated film treatment device that turns exposed areas on a film into areas visible by eye. The device automatically draws in films, washes them with development fluid then dries them. The AGFA model Curix HT-330 film

	processor was used in this project.
Radiochromic film	Photographic film with a sensitive layer of silver halide supported by a gelatine base. When exposed to radiation, the silver halide is broken down and forms crystals of silver which are visible by eye.
Radiographic film	Photographic film made from a radiosensitive polymer that changes colour when exposed to radiation.
Sensitometer	A sensitometer is a light emitting device that can expose film with a range of light intensities and different wavelengths.
Sensitometric curve	See *OD-to-dose curve.*
SFD	See *source to film distance*.
Solid water	Polystyrene $(CH_2)_n$ phantom. It is comprised of sheets 30×30×1 cm^3.
Source to film distance	Source-to-film distance. The distance between the radiation focal point of the linac to the film along a line defined by the central axis of the field.
Source to surface distance (SSD)	Source to surface distance. The distance between the radiation focal point and the top of the phantom.
SSD	See *source to surface distance*.
SW	See *solid water*.
UST	Universal Standardisation Template, a term created for use in this project. A clear template created from joining three Kodak radiographic films together. No exposure was given for each film and then processed, which left behind the clear Base of the film. Three films were chosen because their combined Base made for good transparent properties needed for calibration the Vidar digitiser.
XV	Kodak X-Omat V radiographic film. This is a specific type of radiographic film produced by Kodak.

8 References.

[1] S. Pai, I. J. Das, J. F. Dempsey, K. L. Lam, T. J. LoSasso, A. J. Olch, J. R. Palta, L. E. Reinstein, D. Ritt, E. E. Wilcox, 'Radiographic film for megavoltage beam dosimetry task group 69,' Med. Phys. **34,** 2228-2258 (2007).

[2] G. J. Kutcher, L. Coia, M. Gillin, W. F. Hanson, S. Leibel, R. J. Morton, J. R. Palta, J. A. Purdy, L. E. Reinstein, G. K. Svensson, M. Weller and L. Wingfield, 'Comprehensive QA for radiation oncology: report of AAPM radiation therapy committee task group 40,' Med. Phys. **21,** 581-618 (1994).

[3] B. Fraass, K. Doppke, M. Hunt, G. Kutcher, G. Starkschall, R. Stern and J. V. Dyke, 'AAPM radiation therapy committee task group 53: quality assurance for clinical radiotherapy treatment planning,' Med. Phys. **25,** 1773-1829 (1998).

[4] G. A. Ezzell, J. M. Galvin, D. Low, J. R. Palta, M. B. Sharpe, P. Xia, Y. Xiao, L. Xing and C. X. Yu, "Guidance document on delivery, treatment planning, and clinical implementation of IMRT: Report of the IMRT subcommittee of the AAPM radiation therapy committee," Med. Phys. **8,** 2089-2115 (2003).

[5] International Commission on Radiological Protection, *ICRP publication 60: 1990 recommendations of the International Commission on Radiological Protection*, (Pergamon Press, Oxford, 1991).

[6] P. Winkler, B. Zurl, H. Guss, P. Kindl and G. Stuecklschweiger, 'Performance analysis of a film dosimetric quality assurance procedure for IMRT with regard to the employment of quantitative evaluation methods,' Phys. Med. Biol. **50,** 643-654 (2005).

[7] A. Kapulsky, G. Gejerman and J. Hanley, 'A clinical application of an automated phantom-film QA procedure for validation of IMRT treatment planning and delivery,' Med. Dosim. **29,** 279-284 (2004).

[8] M. Bucciolini, F. B. Buonamici and M. Casati, 'Verification of IMRT fields by film dosimetry,' Med. Phys. **31,** 161-168 (2004).

[9] A. Mack, G. Mack, D. Weltz, S. G. Scheib, H. G. Böttcher and V. Seifert, 'High precision film dosimetry with GAFCHROMIC® films for quality assurance especially when using small fields,' Med. Phys. **30,** 2399-2409 (2003).

[10] B. J. Gerbi and D. A. Dimitroyannis, 'The response of Kodak EDR2 film in high-energy electron beams,' Med. Phys. **30,** 2703-2705 (2003).

[11] N. Dogan, L. B. Leybovich and A. Sethi, 'Comparative evaluation of Kodak EDR2 and XV2 films for verification of intensity modulated radiation therapy,' Phys. Med. Biol. **47,** 4121-4230 (2002).

[12] A. J. Olch, 'Dosimetric performance of an enhanced dose range radiographic film for intensity-modulated radiation therapy quality assurance,' Med. Phys. **29,** 2159-2168 (2002).

[13] C. Martens, I. Claeys, C. De Wagter and W. De Neve, 'The value of radiographic film for the characterization of intensity-modulated beams,' Phys. Med. Biol. **47,** 2221-2234 (2002).

[14] S. G. Ju, Y. C. Ahn, S. J. Huh and I. J. Yeo, 'Film dosimetry for intensity modulated radiation therapy: dosimetric evaluation,' Med. Phys. **29,** 351-355 (2002).

[15] C. Danciu, B. S. Proimos, J. C. Rosenwald and B. J. Mijnheer, 'Variation of sensitometric curves of radiographic films in high energy photon beams,' Med. Phys. **28,** 966-974 (2001).

[16] M. J. Butson, T. Cheung and P. K. N. Yu, 'Radiochromic film dosimetry in water phantoms,' Phys. Med. Biol. **46,** N27-N31 (2001).

[17] J. L. Robar and B. G. Clark, 'A practical technique for verification of three-dimensional conformal dose distributions in stereotactic radiosurgery,' Med. Phys. **27,** 978-987 (2002).

[18] T. Kron, "Dose measuring tools," in *The modern technology of radiation oncology, Vol. 1*, edited by J. Van Dyk, (Medical Physics Publishing, Madison, 1999), pp. 753-821.

[19] J. L. Robar and B. G. Clark, 'The use of radiographic film for linear accelerator stereotactic radiosurgical dosimetry,' Med. Phys. **26,** 2144-2150 (1999).

[20] C. Weltens, D. Huyskens, A. Dutreix, E. Van Der Schueren, 'Assessment of dose inhomogeneities in clinical practice by film dosimetry,' Radiother. Oncol. **49,**287-294 (1998).

[21] A. Niroomand-Rad, C. R. Blackwell, B. M. Coursey, K. P. Gall, J. M. Galvin, W. L. McLaughlin, A. S. Meigooni, R. Nath, J. E. Rodgers and C. G. Soares, 'Radiochromic film dosimetry: recommendations of AAPM radiation therapy committee task group 55,' Med. Phys. **25,** 2093-2115 (1998).
[22] R. L. Stern, B. A. Fraass, A. Gerhardsson, D. L. McShan and K. L. Lam, 'Generation and use of measurement-based 3-D dose distributions for 3-D dose calculation verification,' Med. Phys. **19,** 165-173 (1992).
[23] J. Van Dyk, R. B. Barnett, J. E. Cygler and P. C. Shragge, 'Commissioning and quality assurance of treatment planning computers,' Int. J. Radiat. Oncol. Biol. Phys. **26,** 261-273 (1993).
[24] P. J. Muench, A. S. Meigooni and R. Nath, 'Photon energy dependence of the sensitivity of radiochromic film and comparison with silver halide film and LiF TLDs used for brachytherapy dosimetry,' Med. Phys. **18,** 769-775 (1991).
[25] O. A. Zeidan, D. A. Low and J. F. Dempsey, 'Comparison of small photon beams measured using radiochromic and silver-halide films in solid water phantoms,' Med. Phys. **31,** 2730-2737 (2004).
[26] R. L. Stern, J. Kurylo, C. H. Siantar, J. Lehmann and Z. Goldberg, 'Film dosimetry in the peripheral region using multiple sensitometric curves,' Med. Phys. **31,** 327-332 (2004).
[27] N. L. Childress and I. I. Rosen, 'The design and testing of novel clinical parameters for dose comparison,' Int. J. Radiat. Oncol. Biol. Phys. **56,** 1464-1479 (2003).
[28] M. R. Arnfield, Q. Wu, S. Tong and R. Mohan, 'Dosimetric validation for multileaf collimator-based intensity-modulated radiotherapy: a review,' Med. Dosim. **26,** 179-188 (2001).
[29] J. S. Tsai, D. E. Wazer, M. N. Ling, J. K. Wu, M. Fagundes, T. DiPetrillo, B. Kramer, M. Koistinen and M. J. Engler, 'Dosimetric verification of the dynamic intensity-modulated radiation therapy of 92 patients,' Int. J. Radiat. Oncol. Biol. Phys. **40,** 1213-1230 (1998).
[30] S. Papatheodorou, J. C. Rosenwald, S. Zefkili, M. C. Murillo, J. Drouard and G. Gaboriaud, 'Dose calculation and verification of intensity modulation generated by dynamic multileaf collimators,' Med. Phys. **27,** 960-971 (2000).
[31] J. R. Sykes and P. C. Williams, 'An experimental investigation of the tongue and groove effect for the Philips multileaf collimator,' Phys. Med. Biol. **43,** 3157-3165 (1998).
[32] M. J. Butson, P. K. N. Yu and T. Cheung, 'Rounded end multi-leaf penumbral measurements with radiochromic film," Phys. Med. Biol. **48,** N247-N252 (2003).
[33] T. J. Jordan and P. C. Williams, 'The design and performance characteristics of a multileaf collimator,' Phys. Med. Biol. **39,** 231-251 (1994).
[34] M. S. Huq, I. J. Das, T. Steinberg and J. M. Galvin, 'A dosimetric comparison of various multileaf collimators,' Phys. Med. Biol. **47,** N159-N170 (2002).
[35] B. Mersseman and C. De Wagter, 'Characteristics of a commercially available film digitizer and their significance for film dosimetry,' Phys Med Biol, **43,** 1803-1812 (1998).
[36] I. J. Yeo, C. K. C. Wang and S. E. Burch, 'A filtration method for improving film dosimetry in photon radiation therapy,' Med. Phys. **24,** 1943-1953 (1997).
[37] C. W. Cheng and I. J. Das, 'Dosimetry of high energy photon and electron beams with CEA films,' Med. Phys. **23,** 1225-1232 (1996).
[38] J. H. Killoran, J. Y. Giraud and L. Chin, 'A dosimetric comparison of two multileaf collimator designs,' Med. Phys. **29,** 1752-1758 (2002).
[39] T. Depuydt, A. Van Esch and D. P. Huyskens, 'A quantitative evaluation of IMRT dose distributions: refinement and clinical assessment of the gamma evaluation,' Radiother. and Oncol. **62,** 309-319 (2001).
[40] J. C. P. Heggie, N. A. Liddell and K. P. Maher, *Applied imaging technology*, 4th ed. (St Vincent's Hospital Melbourne, Melbourne, 2001).
[41] I. J. Yeo and J. O. Kim, *A procedural guide to film dosimetry*, (Medical Physics Publishing, Madison, 2004).
[42] G. R. Bird, R. C. Jones and A. E. Ames, 'The efficiency of radiation detection by photographic films: sate-of-the-art and methods of improvement,' Appl. Opt. **8,** 2389-2405 (1969).
[43] S. E. Burch, K. J. Kearfott, J. H. Trueblood, W. C. Sheils, J. I. Yeo and C. K. C. Wang, 'A new approach to film dosimetry for high energy photon beams: lateral scatter filtering,' Med. Phys. **24,** 775-783 (1997).

[44] N. L. Childress and I. I. Rosen, 'Effect of processing time delay on the dose response of Kodak EDR2 film,' Med. Phys. **31,** 2284-2288 (2004).
[45] M. Heydarian, P. W. Hoban and A. H. Beddoe, 'A comparison of dosimetry techniques in stereotactic radiosurgery,' Phys. Med. Biol. **41,** 93-110 (1996).
[46] Å. Palm, A. S. Kirov and T. LoSasso, 'Predicting energy response of radiographic film in a 6 MV x-ray beam using Monte Carlo calculated fluence spectra and absorbed dose,' Med. Phys. **31,** 3168-3178 (2004).
[47] Y. Zhu and J. I. Yeo, 'Portal dosimetry using x-ray film: an experimental and computational study,' Med. Phys. **26,** 2403-2409 (1999).
[48] N. Suchowerska, P. Hoban, A. Davison and P. Metcalfe, 'Perturbation of radiotherapy beams by radiographic film: measurements and Monte Carlo simulations,' Phys. Med. Biol. **44,** 1755-1765 (1999).
[49] J. R. Cunningham, M. Woo, D. W. O. Rogers and A. F. Bielajew, 'The dependence of mass energy absorption coefficient ratios on beam size and depth in a phantom,' Med. Phys. **13,** 496-502 (1986).
[50] M. K. Fix, P. Manser, E. J. Born, R. Mini and P. Rüegsegger, 'Monte Carlo simulation of a dynamic MLC based on a multiple source model,' Phys. Med. Biol. **46,** 3241-3257 (2001).
[51] N. Suchowerska, P. Hoban, M. Butson, A. Davison and P. Metcalfe, 'Directional dependence in film dosimetry: radiographic and radiochromic film,' Phys. Med. Biol. **46,** 1391-1397 (2001).
[52] R. C. Siochi and B. Crawford, 'Pixel value to dose conversion errors can reject acceptable IMRT plans.' Proceedings of the 46th Annual ASTRO Meeting, pp. S625 (2004).
[53] J. Novotny, I. Gomola, J. Izewska, D. Huyskens and A. Dutreix, 'External audit of photon beams by mailed film dosimetry: feasibility study,' Phys. Med. Biol. **42,** 1277-1288 (1997).
[54] M. Oldham, "Radiation sensitive film and gels," in *Handbook of Radiotherapy Physics: Theory and Practice*, edited by P. Mayles, A, Nahum, J.C. Rosenwald, (Taylor & Francis, 2007), pp. 323-324.
[55] T. W. Holmes and E. C. McCullough, 'Acceptance testing and quality assurance of automated scanning film densitometers used in the dosimetry of electron and photon therapy beams,' Med. Phys. **10,** 698-700 (1983).
[56] D. I. Thwaites, B. J. Mijnheer and J. A. Mills, "Quality assurance of external beam radiotherapy," in *Review of radiation oncology physics: a handbook for teachers and students* edited by E. B. Podgorsak (IAEA, Vienna, 2003).
[57] D. A. Low, J. F. Dempsey, J. Markman, S. Mutic, E. E. Klein, J. W. Sohn and J. A. Purdy, 'Toward automated quality assurance for intensity-modulated radiation therapy,' Int. J. Radiat. Oncol. Biol. Phys. **53,** 443-452 (2002).
[58] W. B. Harms, D. A. Low, J. W. Wong and J. A. Purdy, 'A software tool for the quantitative evaluation of 3D dose calculation algorithms,' Med. Phys. **25,** 1830-1836 (1998).
[59] D. A. Low, W. B. Harms, S. Mutic and J. A. Purdy, 'A technique for the quantitative evaluation of dose distributions,' Med. Phys. **25,** 656-661 (1998).
[60] X. Wang, S. Spirou, T. LoSasso, J. Stein, C. S. Chui and R. Mohan, 'Dosimetric verification of intensity-modulated fields,' Med. Phys. **23,** 317-327 (1996).
[61] D. A. Low and J. F. Dempsey, 'Evaluation of the gamma dose distribution comparison method,' Med. Phys. **30,** 2455-2464 (2003).
[62] International Commission on Radiation Units and Measurements, *ICRU report 50. Prescribing, recording, and reporting photon beam therapy*, (ICRU, Bethesda, 1993).
[63] D. W. Anderson and F. St. George, 'Comparison of film and ion chamber systems for depth-dose measurements for a 25 MV beam,' Phys. Med. Biol. **24,** 636-638 (1979).
[64] M. J. Butson, T. Cheung, P. K. N. Yu and M. Currie, 'Surface dose extrapolation measurements with radiographic film,' Phys. Med. Biol. **49,** N197-N201 (2004).
[65] P. Cadman, 'Use of CEA TVS film for measuring high energy photon beam dose distributions,' Med. Phys. **25,** 1435-1437 (1998).
[66] J. Esthappan, S. Mutic, W. B. Harms, J. F. Dempsey and D. A. Low, 'Dosimetry of therapeutic photon beams using an extended dose range film,' Med. Phys. **29,** 2438-2445 (2002).
[67] S. Gotoh, M. Ochi, N. Hayashi, S. Matsushima, T. Uchida, S. Obata, K. Minami, K. Hayashi, T. Matsuo, M. Iwanaga, A. Yasunaga and S. Shibata, 'Narrow photon beam dosimetry for linear accelerator radiosurgery,' Radiother. Oncol. **41,** 221-224 (1996).

[68] J. I. Hale, A. T. Kerr and P. C. Shragge, 'Calibration of film for accurate megavoltage photon dosimetry,' Med. Dos., **19**, 43-46 (1994).
[69] R. D. Lewis, S. J. S. Ryde, A. W. Seaby, D. A. Hancock and C. J. Evans, 'Use of Monte Carlo computation in benchmarking radiotherapy treatment planning system algorithms,' Phys. Med. Biol. **45**, 1755-1764 (2000).
[70] R. Mayer, A. Williams, T. Frankel, Y. Cong, S. Simons, N. Yang and R. Timmerman, 'Two-dimensional film dosimetry application in heterogeneous materials exposed to megavoltage photon beams,' Med. Phys. **24**, 455-460 (1997).
[71] L. J. Van Battum and B. J. M. Heijmen, 'Film dosimetry in water in a 23 MV therapeutic photon beam,' Radiother. Oncol. **34**, 152-159 (1995).
[72] J. F. Williamson, F. M. Khan and S. C. Sharma, 'Film dosimetry of megavoltage photon beams: a practical method of isodensity-to-isodose curve conversion,' Med. Phys. **8**, 94-98 (1981).
[73] X. R. Zhu, P. A. Jursinic, D. F. Grimm, F. Lopez, J. J. Rownd and M. T. Gillin, 'Evaluation of Kodak EDR2 film for dose verification of intensity modulated radiation therapy delivered by a static multileaf collimator,' Med. Phys. **29**, 1687-1692 (2002).
[74] J. Izewska and G. Rajan, "Radiation dosimeters," in *Review of radiation oncology physics: a handbook for teachers and students* edited by E. B. Podgorsak (IAEA, Vienna, 2003).
[75] International Atomic Energy Agency, *TRS 398. Absorbed dose determination in external beam radiotherapy*, (IAEA, Vienna, 2000).
[76] H. E. Johns and J. R. Cunningham, *The physics of radiology,* (Charles C Thomas, Springfield, 1983).
[77] K. S. Krane, *Introductory nuclear physics*, (John Wiley & Sons, New York, 1988).
[78] Y. Wang, P. Cross and W. Zealey, 'An investigation into the source of low energy scattered radiation of significance in film dosimetry,' Aus. Phys. Eng. Sci. Med. **25**, 139-143 (2002).
[79] M. Sastre-Padro, c. Lervåg, K. Eilertsen and E. Malinen, 'The performance of multileaf collimators evaluated by the stripe test,' Med. Dos. **34**, 202-206 (2008).
[80] J. F. Hamilton and L. E. Brady, 'The role of mobile silver ions in latent-image formation,' J. Phys. Chem. **66**, 2384-2396 (1962).
[81] C. Martens, I. Claeys, C. De Wagter and W. De Neve, 'The value of radiographic film for the characterization of intensity-modulated beams,' Phys. Med. Biol. **47**, 2221-2234 (2002).